KTH ROYAL INSTITUTE
OF TECHNOLOGY

Licentiate Thesis in Information and Communication Technology

Mobility Management and Localizability for Cellular Connected UAVs

IRSHAD AHMAD MEER

Stockholm, Sweden 2024

Mobility Management and Localizability for Cellular Connected UAVs

IRSHAD AHMAD MEER

Academic Dissertation which, with due permission of the KTH Royal Institute of Technology, is submitted for public defence for the Degree of Licentiate of Engineering on Friday the 12th April 2024, at 2:00 p.m. in Amiga, Kistagången 16, Kista.

Licentiate Thesis in Information and Communication Technology
KTH Royal Institute of Technology
Stockholm, Sweden 2024

TRITA-EECS-AVL-2024:28
ISBN 978-91-8040-870-7

Printed by: Universitetsservice US-AB, Sweden 2024

Abstract

Unmanned Aerial Vehicles (UAVs) connected to cellular networks present novel challenges and opportunities in mobility management and localization, distinct from those faced by terrestrial users. This thesis presents an integrated approach, combining two key aspects essential for the integration of UAVs with cellular networks.

Firstly, it introduces the mobility management challenges for cellular-connected UAVs, which differ significantly from terrestrial users. While terrestrial mobility management primarily aims to prevent radio link failures near cell boundaries, aerial users experience fragmented and overlapping coverage with line-of-sight conditions involving multiple ground base stations (BSs). Thus, mobility management for UAVs extends beyond link failure avoidance, aiming to minimize unnecessary handovers while ensuring extended service availability, particularly in up-link communication. Line-of-sight conditions from a UAV to multiple BSs increase the likelihood of frequent handovers, resulting in control packet overheads and communication delays. This thesis proposes two approaches to address these challenges: 1) A model-based service availability-aware Mobility Robustness Optimization (MRO) adapting handover parameters to maintain high service availability with minimal handovers, and 2) A model-free approach using Deep Q-networks to decrease unnecessary handovers while preserving high service availability. Simulation results demonstrate that both the proposed algorithms converge promptly and increase the service availability by more than 40% while the number of handovers is reduced by more than 50% as compared to traditional approaches.

Secondly, to assess the ability of a network to support the range-based localization for cellular-connected UAVs, an analytical framework is introduced. The metric B-localizability is defined as the probability of successfully receiving localization signals above a specified Signal-to-Interference plus Noise Ratio (SINR) threshold from at least B ground BSs. The framework, accounting for UAV-related parameters in a three-dimensional environment, provides comprehensive insights into factors influencing localizability, such as distance distributions, path loss, interference, and received SINR. Simulation studies explore the correlation between localizability and the number of participating BSs, SINR requirements, air-to-ground channel characteristics, and network coordination. Additionally, an optimization problem is formulated to maximize localizability, investigating the impact of UAV altitude across different scenarios. Our study reveals that in an urban macro environment, the effectiveness of cellular network-based localization increases with altitude, with localizability reaching 100% above 60 meters. This finding indicates that utilizing cellular networks for UAV localization is a viable option.

Keywords: Unmanned aerial vehicles, Localization, Service availability, Air-to-ground channel, Mobility, Handover

Sammanfattning

Unmanned Aerial Vehicles (UAV) anslutna till cellulära nätverk presenterar nya utmaningar och möjligheter inom mobilitetshantering och lokalisering, skilda från dem som markanvändare står inför. Denna avhandling presenterar ett integrerat tillvägagångssätt, som kombinerar två nyckelaspekter som är väsentliga för integrationen av UAV:er med cellulära nätverk.

För det första introducerar den mobilitetshanteringsutmaningarna för mobilanslutna UAV:er, som skiljer sig avsevärt från markbundna användare. Medan markbunden mobilitetshantering i första hand syftar till att förhindra radiolänkfel nära cellgränser, upplever antennanvändare fragmenterad och överlappande täckning med siktlinjeförhållanden som involverar flera markbasstationer (BS). Mobilitetshantering för UAV sträcker sig sålunda bortom att undvika länkfel, och syftar till att minimera onödiga överlämningar samtidigt som man säkerställer utökad servicetillgänglighet, särskilt i upplänkskommunikation. Synlinjeförhållanden från en UAV till flera BS:er ökar sannolikheten för frekventa överlämningar, vilket resulterar i kontrollpaketkostnader och kommunikationsförseningar. Denna avhandling föreslår två tillvägagångssätt för att möta dessa utmaningar: 1) En modellbaserad tjänsttillgänglighetsmedveten Mobility Robustness Optimization (MRO) som anpassar parametrar för överlämning för att bibehålla hög servicetillgänglighet med minimal överlämning, och 2) Ett modellfritt tillvägagångssätt med Deep Q- nätverk för att minska onödiga överlämningar samtidigt som hög servicetillgänglighet bibehålls. Simuleringsresultat visar att båda de föreslagna algoritmerna konvergerar snabbt och ökar tjänstens tillgänglighet med mer än 40% medan antalet överlämningar minskas med mer än 50% jämfört med traditionella metoder.

För det andra, för att bedöma förmågan hos ett nätverk att stödja den räckviddsbaserade lokaliseringen för de cellulärt anslutna UAV:erna, introduceras ett analytiskt ramverk. Metriska B-lokaliseringsförmågan definieras som sannolikheten för att framgångsrikt ta emot lokaliseringssignaler över en specificerad signal-till-interferens plus brusförhållande (SINR) tröskel från minst B jord BSs. Ramverket, som tar hänsyn till UAV-relaterade parametrar i en tredimensionell miljö, ger omfattande insikter i faktorer som påverkar lokaliserbarhet, såsom avståndsfördelningar, vägförlust, störningar och mottagen SINR. Simuleringsstudier undersöker korrelationen mellan lokaliserbarhet och antalet deltagande BS:er, SINR-krav, luft-till-mark-kanalegenskaper och nätverkskoordination. Dessutom har ett optimeringsproblem formulerats för att maximera lokaliseringsförmågan, undersöka effekten av UAV-höjd över olika scenarier. Vår studie avslöjar att i en urban makromiljö ökar effektiviteten av mobilnätsbaserad lokalisering med höjden, med lokaliserbarhet som når 100% över 60 meter. Detta fynd indikerar att användning av mobilnät för UAV-lokalisering är ett gångbart alternativ.

Keywords: Unmanned aerial vehicles, Localization, Service availability, Air-to-ground channel, Mobility, Handover

Acknowledgements

I would like to extend my sincere gratitude to my main supervisor Cicek Cavdar. Cicek has been my mentor throughout this journey and has provided me with support through my professional and personal challenges. In the face of some of life's most challenging losses and the reception of most beautiful gift from ALLAH, Cicek has consistently extended her support and invaluable guidance. Her influence has been pivotal in shaping my professional trajectory, and I am sincerely thankful for her contributions. Beyond the realm of work, I appreciate Cicek for fostering a sense of belonging within the research group, organizing picnics and lunches that provided opportunities for meaningful connections. From the depths of my heart, thank you, Cicek, for your indispensable role in my journey.

I also want to thank my co-supervisors Mustafa Ozger and Ki Won Sung for their invaluable guidance, insightful feedback, and unwavering commitment to my academic growth. Working under their mentorship has been a truly fortunate experience. A special thanks to my co-authors, Mustafa Ozger and Dominic Schupke for their expertise, creative insights, and dedicated collaboration. This thesis reflects the spirit of teamwork that defined our collective efforts, and I am proud to have co-authored with such talented individuals.

Acknowledgment is due to the CELTIC-NEXT Project, 6G for Connected Sky (6G-SKY) for the financial support that made this research possible. This funding facilitated crucial research activities, conference attendance, and access to essential resources.

I want to express my appreciation to my colleagues at KTH, including Zinat, Ozan, Yasaman, Murtaza, Sara, Milad, Meysam, Satya, Ozlam, Aunas, Yuhang, Shuai, and others. Their encouragement and support have been instrumental in keeping me motivated and resilient through challenges.

Finally, I want to express my deepest gratitude to my family for their steadfast support, boundless love, and unwavering encouragement. I am especially grateful to my wife, Sadaf Ul Zuhra, whose presence has been a true blessing in my life. My brother, Fayaz Ahmad Mir, has been my pillar of strength, providing unwavering support throughout my journey. I also extend my appreciation to my sisters, Rashida and Ruby. Their belief in my abilities and sacrifices laid the foundation for this thesis.

In conclusion, I am deeply grateful for the opportunities and support I have received. I eagerly anticipate continuing my journey in the pursuit of knowledge and academic excellence.

Irshad Ahmad Meer,
Stockholm, Jan 2024

In Grateful Dedication to Zaina,
my Anchor in the Past and Beacon to the Future...

Contents

List of Figures

List of Tables

List of Acronyms

BS	Base station
UAV	Unmanned aerial vehicle
MRO	Mobility robustness optimization
SON	Self organizing network
HOM	Handover margin
TTI	Time to trigger
SINR	Signal to interference plus noise ratio
RSRP	Reference signal received power
RSSI	Received signal strength indicator
DQN	Deep Q-Network
MAC	Medium access control
KPI	Key performance indicators
DNN	Deep neural networks
LOS	Line-of-sight

List of Papers

1. **Availability Oriented Mobility Management for Cellular-Connected UAVs: Model Based Versus Learning Based Approaches** [1]
   I. A. Meer, M. Ozger, D. Schupke, and C. Cavdar
   IEEE Transactions on Network and Service Management, 2024.

2. **Cellular Localizability of Unmanned Aerial Vehicles** [2]
   I. A. Meer, M. Ozger, and C. Cavdar
   Vehicular Communications, Volume 44, 2023.

Other Papers

I participated in several additional projects that are not included in this thesis. However, I have listed the peer-reviewed papers resulting from these projects below for the sake of completeness.

1. **Low-Latency MAC Design for Pairwise Random Networks** [4]
   I. A. Meer, Woong-Hee Lee, Mustafa Ozger, Cicek Cavdar, and Ki Won Sung
   IEEE 95th Vehicular Technology Conference:(VTC2022-Spring), 2022.

2. **D3QN-Based Trajectory and Handover Management for UAV Co-Existing with Terrestrial Users** [5]
   Y. Deng, **I. A. Meer**, S. Zhang, M. Ozger and C. Cavdar
   21st International Symposium on Modeling and Optimization in Mobile, Ad Hoc, and Wireless Networks (WiOpt), Singapore, 2023,

Chapter 1

Introduction

1.1 Background

In the impending future, UAVs, commonly called as drones, are poised to assume a pivotal role in our daily lives [6]. Specifically within the realm of wireless communications, UAVs can serve in three primary capacities: 1) as flying base stations augmenting coverage and capacity [7]; 2) as aerial users linked to terrestrial wireless networks (cellular or WiFi) [1, 2]; and 3) as aerial relays establishing a crucial link between transmitters and receivers [8]. These strides are attributed to notable technological advancements in UAV technology, encompassing control systems, embedded technology, security protocols, and communication mechanisms. The realization of these applications on a broad scale necessitates the resolution of numerous research challenges, with a prominent focus on providing UAVs with efficient means of communication and networking.

This thesis concentrates specifically on functioning of UAVs as aerial users and the accompanying research challenges in communication. When UAVs leverage terrestrial cellular networks for communication, they are referred to as cellular-connected UAVs. Facilitating communication between UAVs and cellular networks introduces new possibilities for UAV applications, including cargo transport, surveillance, multimedia transmission, remote sensing, precision agriculture, traffic monitoring, and rescue operations. Achieving the same quality of service (QoS) as terrestrial users becomes imperative for cellular-connected UAVs. Additionally, these UAVs demand dependable command and control signaling and robust connectivity for the seamless transmission of application-related data.

One of the key research challenges associated with the seamless integration of the cellular-connected UAVs is their efficient mobility management. For the terrestrial user, the handover procedure, as shown in Fig. 1.1, transitions the connection of the user between a serving base station (BS), and a target BS. The user initiates a handover request when it detects that the reference signal received power (RSRP) from the target BS is greater than that from the serving BS by a margin known as

the handover margin (HOM), and this condition persists for a duration called as the time to trigger (TTT). In contrast to terrestrial users, the altitude of a UAV plays a substantial role in determining its connectivity with ground-based BSs. The antenna tilt of these ground BSs contributes to the creation of fragmented and overlapping coverage patterns in the sky. This phenomenon results in the satisfaction of handover conditions more frequently than observed for terrestrial users, leading to unwarranted handovers under current mobility management schemes. Addressing this challenge necessitates the development of innovative mobility management schemes specifically tailored to the distinctive characteristics and requirements of cellular-connected UAVs.

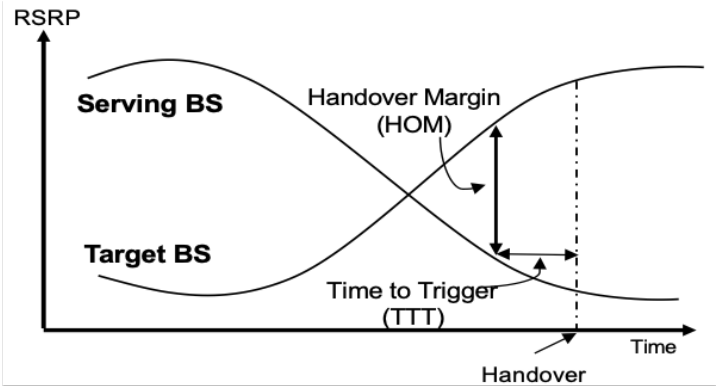

Figure 1.1: Illustration of the user's measurement report on RSRP from the serving and target BS, along with handover parameters: Handover Margin and Time to Trigger.

Since mobility management is responsible for maintaining mobile users' connections as they continue to change their location, it is important that the network has the knowledge of the user locations. The unique advantage of the cellular-connected UAVs having line-of-sight (LoS) channel conditions with multiple ground BSs makes it favorable candidate for range based localization. In range based localization, the target to be localized needs to receive multiple localization signals from different sources. Given cellular-connected UAVs will always be connected with cellular networks, it is possible to utilize cellular BSs as sources in the range based localization of the UAVs. Better localization of the users will allow the network to better map these users for proper resource and mobility management. In the range based localization, target UAV will receive localization signals from multiple surrounding ground BSs and use range combining methods like trilateration, triangulation, or multilateration to calculate the location as shown in Fig. 1.2. The combining method and the number of required signals will depend on the localization technique implemented. Consequently, investigating the cellular network's capability to support range-based localization for UAVs emerges as an intriguing research direction.

In the following, we discuss the primary research questions in this area that this thesis tries to address.

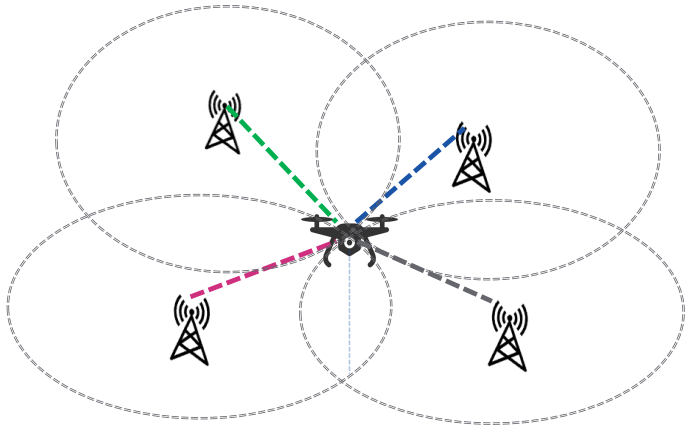

Figure 1.2: Illustration of the signaling process involved in range-based localization for cellular-connected UAVs.

1.2 Research Questions

1.2.1 Service Availability Based Mobility Management

In current mobility management schemes, the decision for handover relies on the relative difference in RSRP between the serving and target BS. However, applying the same method to cellular-connected UAVs, which experience LoS links with multiple ground BSs, can result in unnecessary handovers. These unnecessary handovers in turn lead to additional control packet exchanges between the UAV and the BS, consequently filling the buffer queue and causing delays in the transmission of uplink data. To address this problem, our objective is to refine the handover decision process for cellular-connected UAVs, incorporating not only RSRP but also the buffer queue status of the UAV. For instance, a cellular-connected UAV with excess data in the buffer should prioritize handover to stronger BSs, while a UAV with minimal or no data to transmit should remain with the serving BS as long as the radio link maintains RSRP greater than the minimum threshold.

In addressing this challenge, our research aims to answer the following questions:

RQ1.1: What strategies can be employed to tailor handover decision parameters according to the buffer queue state information of a UAV in a way that optimizes network performance in terms of number of unnecessary handovers and service availability?

RQ1.2: Given the limitations identified in the model-based approach for handovers, what alternative strategies can be explored to directly

base handover decisions on the buffer queue state information of the UAVs?

RQ1.3: How can we translate a handover optimization problem into a reinforcement learning (RL) framework, and what would be an effective modeling approach for defining the action space, state space, and reward structure within this RL context?

1.2.2 Localizability of Unmanned Aerial Vehicles

Exploring the utilization of cellular networks for localizing cellular-connected UAVs represents an exciting research direction. To assess the network's potential in implementing a range-based localization technique for the target, it is crucial to ensure that the target receives sufficient number of usable signals. To gather this information, a new metric must be defined to capture the likelihood of receiving usable signals from a set of ground BSs. Also, to capture the dependence of this metric on the cellular-connected UAVs wireless channel based parameters, an analytical framework needs to be defined and investigated.

In tackling this challenge, our work aims to answer the following research questions:

RQ2.1: How can localizability and associated factors be effectively modeled for UAVs connected with the cellular network?

RQ2.2: In downlink communication-based localization, how does the altitude of a cellular-connected UAV influence its localizability performance, taking into consideration the effects of various network parameters?

RQ2.3: How can the distribution of path loss, interference, and received signal-to-interference-plus-noise ratio (SINR) at the target UAV, particularly with respect to air-to-ground (A2G) channel characteristics, be accurately obtained?

1.3 Related Work

1.3.1 Service Availability Based Mobility Management

We present the current efforts focused on identifying and tackling the challenges associated with mobility management for cellular-connected UAVs. Authors in [9] investigate the effects of altitude of cellular-connected UAVs on coverage and handover performance in terms of radio link failures in urban and rural environments. It is concluded that new network architectures and new mobility management solutions are required to integrate UAVs in 5G and beyond networks. Mobility management is also studied for satellite networks to serve UAVs in [10].

Some of the current studies [11–17] have explored various threshold-based techniques for the mobility management of the cellular-connected UAVs. These studies do not consider the optimization of the handover parameters and are based on

the threshold criteria on the received signal strength indicator (RSSI) or SINR with fixed values of HOM and TTT. However, they improve the UAV mobility management by considering the optimization of UAV speed [17], down-tilt of BS antennas [16], and route of the UAV [11, 12].

Mobility robustness optimization (MRO) has also been explored in recent studies [18–20], where the handover parameters HOM and TTT are optimized based on the quality of experience (QoE), sum capacity and cell load. In [18], authors investigated the optimization of handover parameters for individual terrestrial users using deep Q-network (DQN). Specifically, they explored the use of a service-based QoE metric for optimizing these parameters. The other common approach is to use analytical tools like multi-objective optimization techniques to jointly optimize the key performance indicators such as the number of handovers, spectral efficiency, radio link failure, and outage probability [21].

Machine learning (ML) perticularly RL has found application in the mobility management of wireless networks for both terrestrial and aerial users [17, 22–26]. Several RL-based schemes have been proposed to improve the performance of mobile networks in the context of UAVs. In [22], authors utilized a DQN-based handover decision policy to optimize both handover rate and user throughput. For cellular-connected UAVs, [23] employed Q-learning to minimize handovers and maximize signal quality, proposing an RL-based framework to balance the number of handovers and received signal strength. With the main focus on decreasing the uplink interference from UAVs, authors in [25], proposed an RL-based handover management scheme that jointly optimizes communication delay, interference, and number of handovers in cellular networks. In [26], the authors proposed a handover management scheme based on DQN to strike a balance between signal strength and handover frequency.

Previous works [27–31] on optimizing handover parameters in the MRO has primarily focused on terrestrial users. Our work represents the first effort to devise an MRO mobility scheme tailored specifically to aerial users by optimizing the handover parameters to reduce the number of handovers while improving service availability. Although a Q-learning based MRO scheme was proposed in [19], the authors focused on using UAVs as base stations rather than as aerial users. The ML-powered mobility management schemes proposed for cellular-connected UAVs aim to decrease the number of handovers, but they do not consider the buffer queue state information of the UAVs when making handover decisions. In light of the overlapping coverage encountered by UAVs from ground-based base stations, leveraging buffer queue state information becomes pivotal for the network to make informed handover decisions. This involves efficiently transitioning users with filled buffers to optimize service availability, while concurrently maintaining the association of users with the same base station as long as the link remains stable. The objective is to uphold user service availability and concurrently diminish the frequency of handovers.

1.3.2 Localizability of Unmanned Aerial Vehicles

State-of-the-art range-based localization techniques, encompassing signal strength-based methods such as received signal strength (RSS) or timing-based approaches like time of arrival (TOA) and time difference of arrival (TDOA), offer viable options for UAV localization. The literature presents diverse strategies for UAV localization, as surveyed in [32], particularly focusing on Radio Frequency (RF)-based precise localization techniques tailored for GPS-denied environments. Innovative approaches include utilizing ultraviolet light-emitting diodes on UAVs, as exemplified in [33], and cooperative localization techniques among UAVs, leveraging anchor UAVs to deduce the positions of other UAVs with compromised GPS receivers [34]. Additionally, radar-based systems, requiring both ground radar setups and radar units on UAVs [35], have been explored. Furthermore, [36] proposes employing dedicated sensors on the ground equipped with single or multiple dipole antennas to track target UAVs by receiving RF signals. The main drawback of these methods is that they rely on extra hardware that must be added to UAVs, along with the need for specialized ground setups like cameras and radars. As a result, these requirements make these solutions too expensive for large-scale deployments of UAVs.

The existing literature predominantly addresses the challenge of localizing a generic 3D target using range-based techniques within contexts that focus on enhancing estimation algorithms under favorable channel conditions. Notably, studies such as [37], [38], and [39] assume LoS channel conditions, developing 3D location estimators for RSS and angle of arrival (AOA) range-based techniques. However, these works do not consider the effect of the channel and interference and assume availability of strong decodable signals for accurate estimation from a set sources.

Authors in [40] consider cellular networks for RSS-based localization of the UAVs to calculate the Cramér–Rao lower bound (CRLB). They assume a generic LoS channel model and do not consider localizability before calculating the estimation bounds. In literature, consideration of cellular localizability is limited to terrestrial targets only. Authors in [41] investigate cellular localizability for terrestrial user devices with the help of stochastic geometry. They also show how obtaining a higher number of participating BSs enhances localization precision performance. However, their approach assumes an infinite number of randomly distributed BSs across an unbounded area, an impractical assumption. In [42], authors adopt narrow-band Internet-of-Things (NB-IoT) to study the localizability of the ground sensor nodes. However, they only consider the localization of devices on the ground without considering the challenges of 3D communications. Cellular localizability performance for cellular-connected UAVs is investigated in [43] via simulations by capturing the inherent nature of A2G channels and network dynamics such as interference. However, the statistical characterization of the localizability is missing, which requires a deeper analytical investigation of the path loss, received power, interference, and SINR at the UAV.

In addition to the above two areas, significant advancements have been made in

the field of direct air to ground communication (DA2GC) not only for low-altitude aerial vehicles, specifically UAVs, but also for high-altitude flying vehicles such as airplanes [44–48]. The authors in [46] design an improvised terrestrial network tailored to facilitate DA2GC for airplanes traversing European airspace, with a keen consideration of real-world flight data and traffic patterns. In [47,48], to enhance the onboard connectivity with focus on achieving high-capacity air-to-ground communications, new architecture and gate-to-gate connectivity concepts are introduces. The authors in [49] performed measurement study to utilize directional antenna in connecting the flying vehicles, while in [50], authors use mesh topology to connect flying vehicles. Authors in [51, 52] use an integrate terrestrial and non-terrestrial networks including satellites for improving connectivity for airborne platforms.

1.4 Research Methodology

In Figure 1.3, we present our general research methodology. The research strategy begins by outlining a defined research territory and a very high-level research area. Subsequently, a qualitative literature review is conducted to comprehend the current state of the field, including existing studies and related works. This exploration guides the identification of a specific research gap that aligns with the initial high-level research questions. Throughout this process, continuous verification ensures the meaningfulness of the identified gap and its relevance to practical issues. Following this, a well-defined system model is constructed, accompanied by clear and practical assumptions, and is consistently reassessed alongside the research gap and questions. Once the system model is established, key performance indicators (KPIs) are then defined to evaluate the system. After that, a specific research problem is formulated, with periodic reassessment to ensure clarity. An appropriate evaluation tool is selected to model, analyze, and simulate the network, providing a comprehensive understanding of system behavior and impact of parameters. Based on this understanding, potential improvement opportunities are identified, leading to the proposal of solutions aimed at enhancing network performance. Finally, the proposed solutions are rigorously evaluated to investigate improvements and trade-offs in the network, concluding the research process.

In addressing research questions **RQ1.1** and **RQ1.2** within the domain of network mobility management, our focus centers on exploring how handover decisions affect service availability in terms of the buffer queue state of a UAV. Recognizing the need for novel mobility management solutions to seamlessly integrate UAVs into 5G and beyond networks, we pose the problem of optimizing handover decisions for cellular-connected UAVs. The KPIs in this problem are service availability, queueing delay, and the number of handovers. Two distinct approaches are investigated to address this challenge. The first approach involves a model-based handover parameter optimization scheme known as service availability MRO (SA-MRO). This scheme dynamically adjusts handover management parameters, including HOM and TTT, to optimize service availability. The second approach

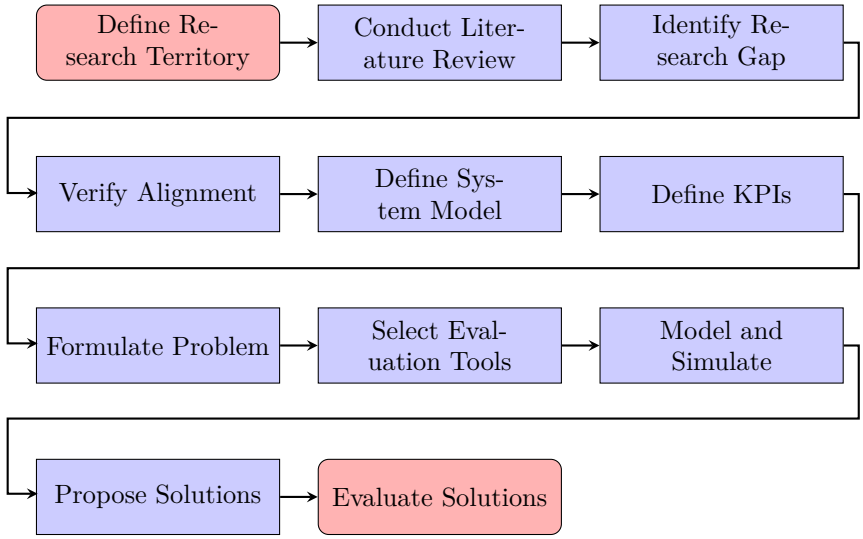

Figure 1.3: Research Methodology

introduces a learning-based handover parameter-free mobility management scheme. Addressing the research question **RQ1.3**, we transformed the optimization problem into the RL paradigm by translating the objective functions into a reward function, and representing the constraints as components within the state and action spaces. In this scheme, a trained DQN agent autonomously makes handover decisions by following a learned policy to guide its actions.

The research area of questions **RQ2.1**, **RQ2.2**, and **RQ2.3** falls within the domain of range-based localization through cellular networks, and the initial question is how to find the ability of the cellular network to be able to localize a UAV through a range-based localization technique. The literature review shows that most studies only consider performance in terms of the accuracy of the localization techniques and do not consider non-deterministic conditions such as network coverage, traffic load, and channel condition on the ability of the network to localize. In our study, we define an analytical framework to quantify the ability of the network to localize a target in 3D. We define the important factors affecting the performance in localizing a UAV in the sky. We formulate an optimization problem to maximize the localizability performance and investigate how altitudes affect localizability. Leveraging tools from stochastic geometry, we derive the distribution of the path loss, interference, and the received SINR by considering UAV-related system parameters in a 3D environment. We perform Monte Carlo simulations and evaluate the results by comparing the simulation results with theory.

1.5 Thesis Contributions

To put our work into the context of current research, an overview of the thesis contributions are listed below:

- **Service Availability Based Mobility Management:**
  Mobility management for terrestrial users is mostly concerned with avoiding radio link failure for the edge users where the cell boundaries are defined. The problem becomes interesting for an aerial user that has fragmented coverage in the sky and experiences LoS conditions with multiple ground BSs. Thus, mobility management is not only about avoiding link failures for the edge user but also avoiding unnecessary handovers while maintaining an extended service availability, especially in the up-link communication. The LoS conditions from a UAV to multiple neighboring BSs make it more prone to frequent handovers, thus leading to control packet overhead and delay in service. The critical nature of UAV missions needs reliable and robust connectivity services, thus making mobility management a critical task for the network. Cellular networks must enable availability-oriented mobility management for aerial communication. Thus the classic MRO procedure optimized for terrestrial users needs to be updated to incorporate aerial users. In this work, we propose the following two approaches for service-oriented availability approach for mobility management of UAVs. 1) A model-based availability-aware MRO where handover control parameters, mainly, HOM and TTT are tuned to maintain high service availability with the minimum number of handovers. 2) A DQN based model-free approach for decreasing unnecessary handovers while maintaining high service availability.

  - **Paper 1:** I. A. Meer, M. Ozger, D. Schupke, and C. Cavdar, “Availability Oriented Mobility Management for Cellular-Connected UAVs: Model Based Versus Learning Based Approaches". IEEE Transactions on Network and Service Management.

- **Localizability of Unmanned Aerial Vehicles:**
  Localization of the cellular-connected UAVs plays an important role in their security and operation. In this area, we focus on the ability of a cellular network to support range-based localization schemes which require more than one detectable signals from the BSs. We propose an analytical framework for B-localizability of UAVs, which is the probability of successfully receiving localization signals above a certain SINR level from at least B ground BSs. Our framework provides a holistic insight into distance distributions of the target UAV, distribution of path loss, interference, and the received SINR by considering UAV-related system parameters in a 3D environment. In our simulation study, we investigate the relation between the localizability and the number of participating BSs, received signal SINR requirements, air-to-ground channel characteristics, and network coordination, which are shown to

be the most important factors for the localizability performance of UAVs. We formulate an optimization problem to maximize the localizability performance and investigate how altitudes affect the localizability for different scenarios.

- **Paper 2:** I. A. Meer, M. Ozger, and C. Cavdar, “Cellular Localizability of Unmanned Aerial Vehicles". Elsevier Vehicular Communications, Volume 44, 2023.

1.6 Thesis Outline

The rest of this thesis is organized as follows. In Chapter 2, we investigate the service availability based mobility management and propose two handover optimization algorithms to minimize the number of handovers while improving the service availability. In Chapter 3, we consider the localizability of the cellular-connected UAVs and investigate the impact of network coverage, traffic load, and channel condition on the localizability performance. Concluding remarks and future research directions are given in Chapter 4. Finally, the dissertation concludes with the appended papers at the end, offering additional depth and context to the presented research.

Chapter 2

Service Availability Based Mobility Management

Different from terrestrial users, flexibility by 3D movement of cellular-connected UAVs and undefined cell boundaries in the sky makes mobility management a more challenging task. The altitude in 3D operation of UAVs has a profound impact on association of the UAV as a farther BS may possibly be chosen as the serving BS over the closest BS. This is because, the BS antennas are tilted downwards to optimize terrestrial coverage and UAVs at some altitude may be served by the sidelobes of the BS antennas. This means, unlike a terrestrial user which experiences strong signals from nearest BSs only, aerial users may experience an antenna null from the nearest BS and a strong signal from the farther BS. This leads to fragmented and overlapping coverage from different BSs in the sky. It is shown that due to the fragmented BS association pattern in the sky, a large number of handovers are observed from measurement studies in LTE networks [53, 54], and [55]. The frequent unnecessary handovers while serving UAVs adds the control data leading to the increased packet delay. In order to have the UAV data transmitted with low latency and with more reliability, future cellular networks need to upgrade the mobility management schemes to effectively manage mobility of UAVs in 3D .

Most of the UAV applications like surveillance, remote sensing, precision agriculture, traffic monitoring, and rescue operations require to upload the data with the minimum possible delay. The service-related data in the buffer queue can experience long wait time because of the excess control data generated due to the multiple handovers. The data is correlated with the location of the UAV and because of the high mobility of the UAVs, the delayed data in the buffer queue can become obsolete and thus severely affecting the service availability.

From aerial networks perspective, communication reliability is defined as the probability that an end-to-end message is transmitted within a certain time limit [56]. This definition also considers the service availability, defined as the percentage of time the network delivers the required service. In this work, to realize the use

cases of the UAVs, we define the performance metric capturing the buffer queue data of the cellular-connected UAVs. We define the **service availability** as the probability that the buffer queue length is smaller than a predefined threshold. The outage means that the packets delayed in the buffer become obsolete and will lead to the service unavailability. This definition captures different dimensions of the communications such as user buffer, data rate and resulting delay for the transmitted packets.

In this work, we propose two novel service availability oriented mobility management schemes for aerial users. In the first approach, a service availability oriented MRO algorithm is proposed to dynamically update the handovers parameters such as HOM and TTT. However, unlike previous approaches on the MRO which consider signal strength based performance for updating the handover parameters, the proposed scheme adds service availability as a constraint to the MRO for optimizing the handover parameters. The model based approach is threshold based and depends on handover parameters in the network and their optimization is limited with the parameter space. We aim to adopt a handover parameter free approach for mobility management. Machine learning provides such an opportunity to develop a mobility management scheme which does not depend on the handover parameters and has a larger optimization space. Therefore, we propose a service availability oriented learning based mobility management algorithm which combines deep neural networks (DNN) and reinforcement learning (RL) for taking the handover and resource allocation decisions. The RL-based mobility management scheme aims to optimize KPIs such as service availability, delay and number of handovers for cellular-connected UAVs. The two approaches solving the same problem are different in many ways as the former is a model based approach while later is model free learning based approach. The resulting approaches are compared with the benchmark scheme with a fixed HOM and TTT and the results are validated in a dynamic system-level simulations implementing a realistic 3GPP aerial user scenario from [53]. The main contributions of this study can be summarized as follows:

- Uncovering the challenges in mobility management in 3D communication using the traditional schemes.

- A model based adaptive handover scheme to increase the service availability while decreasing the number of handovers by adopting the HOM and TTT based on the RSSI and UAV status i.e., buffer queue length information.

- A learning based approach for mobility management to increase the service availability while decreasing the number of handovers by taking the handover decisions based on the current state which includes UAV current location and buffer queue length information.

- Implementation and validation of the proposed algorithms via dynamic system level simulations using a realistic 3GPP aerial user scenario from [53].

2.1 System Model

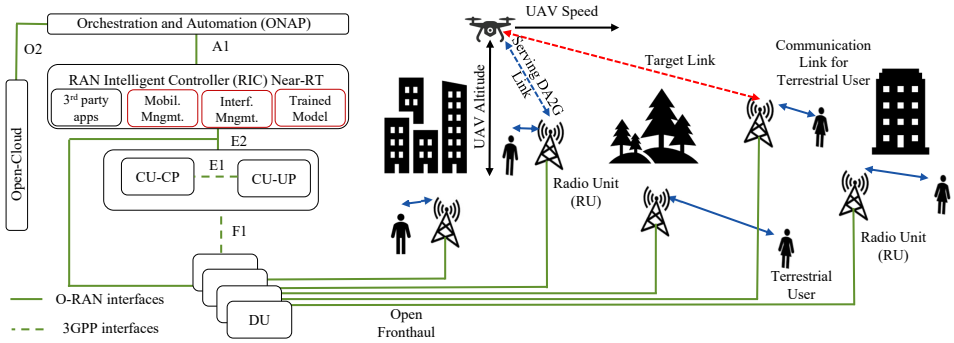

Figure 2.1: Network Architecture (Reprinted from [1], ©2024 IEEE, reused with permission).

Throughout this work, we consider the following UAV up-link communication scenario (i.e., from the UAVs to BSs), which is depicted in Fig. 2.1. In a given service area, we have a total of N BSs deployed at fixed locations. A total of K UAVs are moving inside of the area at the same time, and they are being served by the BSs on orthogonal resource blocks. We assume that the network has the location information of the UAVs moving in the service area. We consider for any UAV k, $\mathcal{L}_k \in N$ is the set of closest neighboring candidate BSs for the handover. The BSs operate in a total bandwidth $\mathbb{B}$ consisting of N_b radio resource blocks (RRBs). The serving direct air to ground (DA2G) link for the UAV is shown by the blue dashed line and communication links for terrestrial users are depicted by dashed green lines in Fig. 2.1. The target BS DA2G link is shown by the red dashed line in Fig. 2.1. The UAV will handover to a target BS, if it satisfies the handover condition i.e., having signal strength from the target BS greater than the serving BS by a margin greater than the HOM. We assume that the connection with the source BS remains unchanged during the establishment of the connection with the target BS, which is referred to as a soft handover. This procedure does not have an impact on the handover decision-making but it improves the connection continuity.

Fig. 2.1 details the presented architecture for mobility management decisions, which utilizes open radio access network (O-RAN) architecture focusing on O-RAN Alliance standards as our reference. O-RAN provides openness through open interfaces to enable customization of the network and intelligence at every layer of the network to enable optimized closed-loop automation [57]. Disaggregation in O-RAN enables to divide BSs across multiple nodes in the RAN [58]. Hence, BSs are logically separated into different nodes for RAN functionalities which are radio units (RUs), distributed units (DUs), central unit-user plane (CU-UP), and central unit-control plane (CU-CP). These units are connected through interfaces defined by O-RAN and 3GPP. The green bold connections represent O-RAN interfaces

whereas the dashed green connections show 3GPP interfaces in Fig. 2.1. RUs are connected to DUs via open fronthaul links, and DUs are connected to the CU over the F1 interface. The E1 interface connects the user and control plane at the CU. One important feature of O-RAN is the new functionality named Radio Intelligent Controller (RIC). RIC Near Real-Time (Near-RT) layer provides intelligent radio resource management, and quality of service management [57]. It also can leverage intelligence in RAN functions such as quality of service management, connectivity management, and seamless handover management [57]. RIC Near-RT is connected with RAN via the E2 interface to control the aforementioned functionalities. A1 is the interface connecting the orchestration and automation layer and the RIC Near-RT layer. Open-Cloud consists of pooled resources for computing and virtualization infrastructure from one or several data centers [59]. The interface that connects the management and orchestration functionalities with the cloud is the O2 interface.

The learning-based approach is implemented within the network at the RIC layer, as highlighted in red in Fig. 2.1. This placement allows for centralized training, with execution distributed across users. By leveraging centralized resources for training and distributed execution per user, our design aims to efficiently meet the computational complexity demands of the deep neural network model and ensure a balance between efficiency and scalability. Furthermore, this architecture has handover management functionalities that can also support MRO as a part of SONs for our model-based approach.

2.1.1 Air-to-Ground Channel

We follow the DA2G channel model for urban environments provided in [53]. For the suburban and rural areas, we can use the same channel model with the simple substitution of respective parameters. We use probabilistic path loss models for the DA2G channels with separate LoS and non-LoS links. According to [53], at time slot t, the probability of experiencing LoS propagation in the communication link between the lth BS and the UAV at altitude h with a flying speed of v is calculated as follows:

$$\mathcal{P}_{\text{LOS}} = \begin{cases} 1, & d^l_{\text{2D}} \leq d_1 \\ \dfrac{d_1}{d^l_{\text{2D}}} + \exp\left(\dfrac{d_1}{p_1}\right)\left(1 - \dfrac{d_1}{d^l_{\text{2D}}}\right), & d^l_{\text{2D}} > d_1 \end{cases}, \tag{2.1}$$

where $p_1 = 4300\log_{10}(h) - 3800$, $d_1 = \max\big((460\log_{10}(h) - 700), 18\big)$, in meters, and d^l_{2D} is the horizontal or 2D distance between the UAV and the BS l for $22.5 < h \leq 100$ (in meters). For $100 < h \leq 300$, $\mathcal{P}_{\text{LOS}} = 1$ is assumed. For LoS condition, the path loss PL_{LOS}, when $22.5 < h \leq 100$, is given as [53]:

$$\text{PL}_{\text{LOS}} = 28 + 22\log_{10}(d_{\text{3D}}) + 20\log_{10}(f_c), \tag{2.2}$$

where d^l_{3D} is the 3D distance between the UAV and the lth BS in meters, h_{BS} is the height of the BS, and f_c is the carrier frequency in GHz. Path loss for non-LoS

(NL) condition, $\mathrm{PL_{NL}}$, is given as [53]:

$$\mathrm{PL_{NL}}=15+\big(46\text{-}7\log_{10}(h)\big)\log_{10}(d_{3\mathrm{D}})+20\log_{10}(f_c). \tag{2.3}$$

Shadow fading also depends on the LoS/NL condition. Standard deviation of the shadow fading for LoS condition is $\sigma_{\mathrm{LOS}} = 4.64\ \exp(-0.00066h)$, and for NL condition, $\sigma_{\mathrm{NL}} = 6$ [53].

We consider UAVs with a single omnidirectional antenna. For BSs, we assume a vertical N-element uniform linear array (ULA), where each element is omnidirectional in azimuth with a maximum gain of g_E^{max}. Directivity as a function of the zenith angle is given by the following [60]:

$$g_E(\Theta) = g_E^{max}\sin^2(\Theta), \tag{2.4}$$

where Θ is the zenith angle between the ground BS and the UAV. Considering half-wavelength spacing between the adjacent antenna elements and a fixed down-tilt angle Θ_t, the array factor of the ULA is calculated as

$$g_A(\Theta) = \frac{\sin^2(N\pi(\cos\Theta-\cos\Theta_t)/2)}{N\sin^2(\pi(\cos\Theta-\cos\Theta_t)/2)}. \tag{2.5}$$

The BSs antenna gain in linear scale is calculated as

$$g(\Theta) = g_E(\Theta)\times g_A(\Theta). \tag{2.6}$$

2.1.2 Buffer Queue and Traffic Model

Many UAV applications, especially for surveillance applications need to have low delay communication to send observed data such as video. Therefore, one of the main focuses of this paper is the up-link communication delay for UAVs. Let $u(t)$ denote the number of data units in bits that arrive at the buffer of the UAV at the end of time epoch t. The data units arriving in the buffer follow the Poisson point process (PPP) distribution with a mean arrival rate of λ_k^0 for UAV k. Since the handover decision needs some control packets to be transmitted, the handover decision affects the arrival rate of control data units. Taking this into consideration, we model the arrival rate of data units to the buffer queue of UAV k as follows:

$$\lambda_k(t) = \lambda_k^0 + \sum\nolimits_{\tau=1}^{T_h} I(k,t-\tau)\lambda_{k,h}^m, \tag{2.7}$$

where $\lambda_{k,h}^m$ models the arrival rate of control signals due to handover, T_h represents the length of time for which control messages will be issued after a handover decision, and $I(k,t-\tau)$ is a handover indicator function, which is equal to one if a handover occurred for UAV k at $t-\tau$, and zero otherwise. Due to the handovers and associated control signal arrivals, we have light and heavy traffic arrival windows and to model both application and control data, we follow a Switched PPP

(SPP) model. If $q_k(t)$ represents the number of data units at the start of the time epoch t in the buffer queue of the UAV k. During the transmission interval, the transmitted (served) data from the queue is given by $s_k(t)$ the arrived data to the queue is given by $u(t)$. Hence, UAV k's buffer queue size (or buffer queue state information) as one of our KPI is modeled as

$$q_k(t+1) = \left[q_k(t) + u_k(t) - s_k(t)\right]^+, \tag{2.8}$$

where $[x]^+ = max(x, 0)$ indicates that the amount of served data cannot exceed the amount of the stored data in the queue. The newly arriving packets at time t will experience a queuing delay of $q_k(t)/R_k(t)$ where $R_k(t)$ is the expected data rate for UAV k. We assume an upper limit on the buffer queue size, i.e., $q_k^{\max}$, beyond which a packet is dropped.

2.1.3 Allocated Spectrum and Data Rate

To calculate the up-link data rate for UAV k, we assume that the transmission time interval (TTI) is less than the coherence time of the channel. Therefore, the data rate over the allotted sub-carriers, denoted by $\mathbf{b}_k(t)$ is derived as:

$$R_k(t) = \mathcal{F}(W_s, \mathbf{b}_k(t), \mathbf{p}_k(t), \mathbf{h}_k(t)), \tag{2.9}$$

where $\mathcal{F}(\cdot)$ is a function, to be described in the following. Furthermore, W_s is the sub-carrier bandwidth, $\mathbf{p}_k(t)$ is the power allocation vector, $\mathbf{h}_k(t)$ is the vector of the ratio of channel gains to the noise plus interference level over the allocated set of sub-carriers. Without loss of generality, we exemplify our modeling for single carrier frequency division multiple access and approximate the $\mathcal{F}(\cdot)$ function as:

$$\mathcal{F}(W_s, \mathbf{b}_k(t), \mathbf{p}_k(t), \mathbf{h}_k(t)) \approx W_s |\mathbf{b}_k| \log_2(1 + \gamma_k(t)), \tag{2.10}$$

where,

$$\gamma_k(t) = P_k \cdot g_k(\Theta, t) \left(\sum_{s \in \mathbf{b}_k(t)} \frac{1}{\alpha_{s,k}(t)} \right)^{-1}; \tag{2.11}$$

$$\alpha_{s,k}(t) = \frac{|H_{s,k}(t)|^2}{N_0 + W_s I_{s,k}(t)}; \tag{2.12}$$

N_0 is the noise power over each subcarrier; $I_{s,k}(t)$ is the power density of interference over the sth subcarrier; P_k is the transmit power; $g_k(\Theta, t)$ is the antenna gain; and $H_{s,k}(t)$ is the frequency-domain channel response of the sth subcarrier and includes path loss, shadowing, and multipath fading [61]. Furthermore, $\mathbf{b}_k(t)$ is characterized by a RRB allocation indicator function, denoted by $\Phi(l, b, t, k)$, which is 1 if the b RRBs of BS l is allocated at time t to the kth UAV and 0 otherwise.

The decision of the handover at any time epoch, denoted as t, impacts the data rate as expressed in (2.10) in two ways. Firstly, it affects the channel response to

the newly associated BS, resulting in a change in data rate. Secondly, the impact due to the allocated number of RRBs, is represented by $|\mathbf{b}_k|$. A higher allocation of RRBs correlates with an improved data rate. However, due to resource constraints at the BS, achieving maximum RRB allocation is not always feasible. The change in the data rate affects the buffer queue size, given that the transmitted data $s_k(t)$ equals the product of the data rate and TTI. This, in turn, influences the queueing delay.

2.1.4 Service Availability Model

From an aerial network perspective, service availability is part of communication reliability which is defined as the probability that an end-to-end message is transmitted within a certain time limit [56, 62]. These performance metrics are mainly used for communications regarding airspace management, which includes applications such as air traffic management (ATM), universal traffic management (UTM), remote piloting operations (RPOs), fully autonomous operations, and reduced crew operations. Communication reliability requirements for these operations are given in Table 2.1. These communication demands focus primarily on command and control functionalities. On the other hand, satisfying the requirements of data or payload communication of cellular-connected UAVs is vital to realize use cases. Service availability as one of our main KPIs is defined based on the buffer queue state information of the UAV and is directly affected by the handover decisions. Service availability is achieved if the queue size at the transmitting UAV remains less than the threshold. This is formally defined as:

$$\mathbf{Pr}(q_k(t) \leq q_0) = \delta(t) \quad \forall\, k \in \mathcal{K}, \forall t. \tag{2.13}$$

It is also important that we guarantee queue stability and keep the outages low. These are formally defined as:

$$\mathbb{E}[q_k] = \lim_{T\to\infty} \frac{1}{T} \sum_{t=1}^{T} q_k(t) < \infty \quad \forall\, k \in \mathcal{K}, \tag{2.14}$$

$$\mathbf{Pr}(q_k(t) > q_0) = 1 - \delta(t) \quad \forall\, k \in \mathcal{K}, \forall t, \tag{2.15}$$

where $\mathbb{E}[q_k]$ is the expected buffer queue size for the kth UAV, q_0 is the queue threshold and $1 - \delta(t)$ gives the outage probability. The extreme cases of having queue sizes very long lead to the worst queuing latency and can degrade performance [63].

2.2 Problem Formulation and Solution Approaches

2.2.1 Problem Formulation

In this work, we optimize the handover decisions for the cellular-connected UAVs with an aim to improve service availability, while decreasing the queueing delay,

Table 2.1: Communication Requirements

Application	**Latency**	**Service Availability**	**Ref.**
ATM	5 sec	99.9999%	[64, 65]
UTM	500 ms	99.999%	[64]
RPOs	1-250 ms	99 – 99.99%	[56]

and the number of handovers. For all $k \in K$ and $l \in \mathcal{L}_k$, the set of available RRBs at BS l, at time t is denoted by $\mathcal{B}_l(t)$. Our problem is to reserve b RRBs from BS l at time epoch t to UAV k, which is denoted by $\Phi(l, b, t, k)$. The decisions must improve service availability (or minimize the outage probability) of the UAV with a minimum number of handovers, and minimum queueing delay experienced by the UAV. Then, at decision epoch t, we need to solve the following optimization problem for serving kth UAV:

$$\min_{\Phi} \left[\xi_{\mathrm{r}}(1-\delta_{\mathrm{k}}(t)) + \xi_{\mathrm{d}}(\frac{q_k(t)}{R_k(t)}) + \xi_{\mathrm{h}} I(k,t)\right], \tag{2.16}$$

subject to:

$$(\mathbf{C1})\ \sum\nolimits_{l\in\mathcal{L}} \mathcal{I}\Big(k, 0 < \sum\nolimits_{b\in\mathcal{B}_l(t)} \Phi(l,b,t,k)\Big) = 1,\ \forall k,$$

$$(\mathbf{C2})\ q_k(t) \le q_k^{\max},\ \forall k;$$

$$(\mathbf{C3})\ \sum_{b\in\mathcal{B}_l(t)} \Phi(l,b,t) \le b_l^{\max},\ \forall k;$$

where the term $(1-\delta_k(t))$ represent outage, $\frac{q_k(t)}{R_k(t)}$ represents delay and $I(k,t)$ represents the handover. All the terms in (3.26) are multiplied by the real positive scaling coefficient represented as ξ_r, ξ_d, and ξ_h for service availability, experienced delay, and handover indicator, respectively. Furthermore, $I(k,t)$ is a binary indicator equal to one if a handover has happened for UAV k at time t otherwise zero. The first constraint **(C1)** assures that a UAV is associated with only one BS, **(C2)** ensures that the buffer queue is not overflowing, and **(C3)** states that the available number of RRBs at the BS can not be greater than the maximum number of RRBs of the BS. Furthermore, in the joint-optimization in (3.26), the first term and the second term are correlated but achieve two objectives. The first term in (3.26) aims to minimize the instances where the buffer queue size is greater than the threshold while the second term aims to minimize the queuing delay by efficiently allocating the resources.

2.2.2 Solution Approaches

2.2.2.1 Model based approach

A well defined model based approach for mobility management is based on comparing the received signal power levels between the serving BS and the target BS. The criteria for handover is the difference between the power levels being greater than HOM also known as the hysteresis value for a time interval greater than TTT. After assigning radio resources to the randomly generated terrestrial users, the remaining available radio resources are assigned to the UAV. The UAV using pilot signals sends the measurement report containing the signal strengths from other BSs to the serving BS. The handover is initiated at time τ if the criteria for the handover is met, i.e., if the received signal from a target BS l', $\forall l' \in \mathcal{L}$ is greater than the serving BS l, $\forall l \in \mathcal{L}$ by a HOM of $\Psi(t)$ for a TTT greater than $\Omega(t)$. Therefore, handover is initiated when:

$$P_{k,l'}(t) - P_{k,l}(t) \geq \Psi(t) \quad \forall t \in [\tau - \Omega(t), \tau], \tag{2.17}$$

where $P_{k,l'}(t)$ and $P_{k,l}(t)$ are the pilot signal strengths from the target BSs l' and the serving BS l respectively to the UAV k. The received signal strengths in (2.17) is calculated by taking into account the channel gains, small-scale fading, and antenna gains. The selection of handover parameters is important for optimizing mobility performance, especially for cellular-connected UAVs. If the HOM is too low, it will lead to frequent handovers. When it is too high, it may create extra delay and affect the service availability. The model based approach in (2.17) is dependent on two key handover parameters (HOM and TTT). We design an algorithm that adapts the handover parameters based on the buffer queue size of the UAV i.e., $\Psi(t) = \mathcal{F}(q_k(t))$ and $\Omega(t) = \mathcal{F}(q_k(t))$. Tuning these parameters in an adaptive manner based on the buffer queue size ensures service oriented availability. A complete algorithm on how the parameters are optimized in time is provided in detail in the next section.

2.2.2.2 Learning based approach

In the learning based approach, we do not control the handover parameters for deciding the handover but learn a policy to choose the BS with which the UAV should be connected at each time. This makes the approach model free and it can assign radio resources based on past experience in addition to selecting the serving BS. A solution to the formulated problem in (3.26) at time epoch t affects different performance indicators in future epochs. For instance, a decision for handover propagates in time, which may lead to the ping-pong effect and unnecessary interference to terrestrial users. Furthermore, the optimization problem is highly complex due to the dependencies between decisions taken at different time epochs, non-convex functions, and integer constraints. We transform this problem where we consider the long-term benefits with temporal availability measures. Also, due to the dynamic nature of the cellular network environment, and the changing number of active BSs and terrestrial users, the solution needs to be more adaptive to

the changes in the environment. Hence, to balance between the instantaneous and long-term availability measures, we transform this optimization problem into a RL problem. For this transformation, the constraints from the network are converted into action and state spaces, while the reward function is a transformation of the objective function that we aim to maximize. The goal of the learning problem is defined in the reward function which controls the actions of the agent. Hence, the transformed problem is completely described by the action space, the state space, and the reward function. The central agent responsible for mobility management is trained by running multiple flights of the UAV over the serviced area. We adopt a DQN based algorithm with a decaying learning rate to determine the BS association for the UAV.

2.3 Service Availability Oriented 3D Mobility Management

2.3.1 Proposed SA-MRO Algorithm

The model based SA-MRO algorithm automatically tunes the handover parameters such as HOM (Ψ) and TTT (Ω) as explained in Section 2.2.2.1. During the flight of the UAV, the serving BS connected with a self-organizing networks (SON) entity, collects the data from the UAV and periodically optimizes the handover parameters. The proposed SA-MRO scheme not only aims to reduce unnecessary handovers, and ping-pong rates but also aims to satisfy the service availability constraint. The network starts with the initial values of HOM $\Psi = 2$ dB and TTT $\Omega = 10$ TTI. The UAV sends the buffer queue state information i.e., $q(k)$ to the serving BS in addition to the other information like the signal strength from other BSs. The network after every T_w TTIs calculates the service availability as given in (2.15). The resulting service availability value and the current HOM and TTI determine the updates to the HOM and TTI values. If the service availability is greater than the required ($\delta_{th} = 0.99$) and the HOM is less than the maximum ($\Psi_{max} = 7$ dB), HOM is increased by a value $\Delta(\Psi) = 0.5$ dB and if the HOM is maximum, TTT is increased by $\Delta(\Omega) = 10$ TTIs. The updated values are valid for the next T_w TTIs. The algorithm after every T_w TTIs continues to check whether the service availability requirement is met. If it is satisfied, the algorithm increases the HOM and TTT to reduce the number of handovers. If the service availability requirement is not satisfied, the algorithm decreases the HOM and TTT to let the handover happen to get associated with the better BS. Algorithm 1 summarizes the overall proposed procedure.

The service availability oriented MRO requires continuous measurement reports to be sent to the serving BS. Thus the resulting control packets will lead to further delay. Also, the achievable availability is directly affected by the length of the T_w. Therefore, we look for another solution that can overcome these outcomes.

Algorithm 1 Service Availability Oriented MRO Algorithm

Initialize Ψ, Ω and T_w
while $q_k(t) > 0$ **do**
  if $t \bmod t_w == 0$ **then**
    Obtain the $q_k(t)$, $\Psi(t)$, $\Omega(t)$
    Calculate service availability $\delta_k(t)$
    if $\delta_k(t) \geq \delta_{th}$ and $\Psi < \Psi_{max}$ **then**
      $\Psi(t+1) = \Psi(t) + \Delta(\Psi)$ dB
    else if $\delta_k(t) \geq \delta_{th}$ and $\Psi = \Psi_{max}$ **then**
      $\Omega(t+1) = \Omega(t) + \Delta(\Omega)$ TTI
    else if $\delta_k(t) < \delta_{th}$ and $\Psi > \Psi_{min}$ **then**
      $\Psi(t+1) = \Psi(t) - \Delta(\Psi)$ dB
    else if $\delta_k(t) < \delta_{th}$ and $\Psi = \Psi_{min}$ **then**
      $\Omega(t+1) = \Omega(t) - \Delta(\Omega)$ TTI
    end if
  end if
end while=0

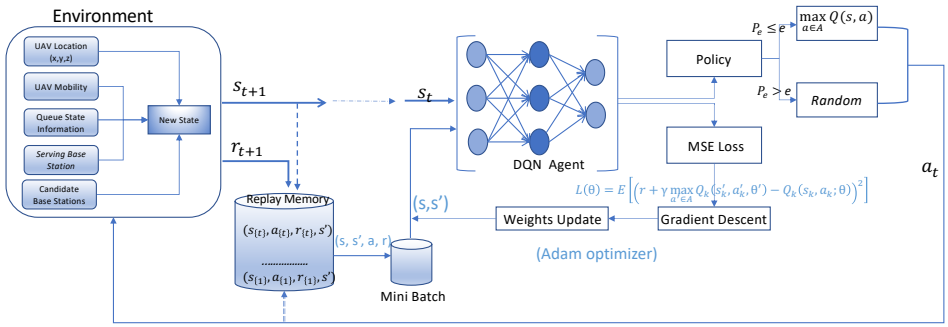

Figure 2.2: Deep Q-Network Architecture (Reprinted from [1], ©2024 IEEE, reused with permission).

2.3.2 Proposed Learning Based Algorithm

We introduce a model-free DQN algorithm, that combines the Q-Learning algorithm and deep neural networks. The DQN leverages experiences to iteratively enhance system performance. In the DQN framework, an agent engages with the environment through a sequence of events, selecting actions from the permissible set and collecting rewards for each action taken. The triple ($\mathcal{S}$, $\mathcal{A}$, r) defines an RL problem, where $\mathcal{S}$ and $\mathcal{A}$ encompass the set of possible states and actions, respectively, and the agent aims to accumulate r as a reward. Fig. 2.2 illustrates the DQN architecture, while Algorithm 2 provides a detailed description. For our specific problem, the DQN-based learning framework is defined as follows:

1) The State Space: It describes the set of all the states accessible to the agent upon executing an action within the specified environment. The discrete state is characterized by factors influencing handover decisions in a given radio environment. In our context, the state of the environment for UAV k at time t is denoted as $S_k(t) = (h_k(t), v_k(t), l_k(t), q_k(t), x_k(t), y_k(t), C_k(t))$, encapsulating altitude, velocity, current serving BS, buffer queue size, the x-axis and y-axis coordinates, and set of strongest candidate BSs of UAV k respectively. If $l_k(t)$ is serving BS, then the number of BSs in $C_k(t)$ will be equal to $(|\mathcal{L}| - 1)$. Consequently, the state space $\mathcal{S}$ encompasses all feasible instances of $S_k(t)$. For instance, $S_k(t) = [100, 20, 1, 0, 100, 200, \{3, 7, 8\}]$ represents a state where UAV k flies at an altitude of 100 m with a speed of 20 m/s, located at $(100, 200)$, served by BS-1, possessing an empty buffer queue, and BS-3, BS-7, BS-8 being the strongest candidate BSs. To limit the number of states, we quantize the area into small squares, each square center representing the x and y coordinates of a specific state.
2) The Action Space: The action space presents the set of decision parameters available to the agent at each decision epoch. We present the action at time t for UAV k as $A_k(t)$=$[\Phi(l, b, t, k)]$, where Φ stands for BS association and radio resource allocation. The action space, $\mathcal{A}$, consists of different combinations of associated BS, and an allocated set of RRBs. For example, $A_k(t) = [\{1, 2\}]$ represents an action in which, UAV k should transmit its data over two chunks of radio resources in BS indexed as 1.
3) The Reward Function: It defines the objective function of the learning based service availability oriented mobility management problem that is to be maximized. Using the notation presented above, the immediate reward for the UAV k at time t, i.e. $r_k(t)$, is defined as a weighted sum of the rewards from service availability, low-delay performance, and a low number of handovers. Hence, we formulate $r_k(t)$ as:

$$\begin{aligned} r_k(t) =& \alpha_{\mathrm{r}} \times \text{Service availability reward} + \alpha_{\mathrm{d}} \times \text{Low-delay} \\ & \text{reward} - \alpha_{\mathrm{h}} \times \text{Handover regret}, \qquad (2.18) \\ =& \alpha_{\mathrm{r}} \delta(k, t) + \frac{\alpha_{\mathrm{d}}}{1 + q_k(t+1)} - \alpha_{\mathrm{h}} I(k, t), \qquad (2.19) \end{aligned}$$

where, α_{r}, α_{d}, and α_{h} are the weights, which are real positive numbers. The weights determine the relative importance of the KPIs in target UAV applications. Definitions of rewards and regrets for respective terms are given in (2.18). In the first term in $r_k(t)$, the service availability reward is obtained when the buffer queue size is less than a threshold. The second term, Low-delay reward, is proportional to the inverse of buffer queue size, and finally, the last term, handover regret, is an indicator of a handover event, and hence, its contribution is negative in the immediate reward. The first term and the second term in (2.19) are correlated but achieve two objectives. The first term in (2.19) aims to reward the instances where the buffer queue size is lesser than the threshold while the second term aims to reward for reducing the queuing data and thus delay by efficiently allocating the

resources. Furthermore, all these measures have been scaled in $[0, 1]$ interval, to prevent any one metric from dominating others.

$$Q_k(s_k, a_k; \theta) = r + \gamma \max_{\mathbf{a}' \in \mathcal{A}} Q_k(s'_k, a'_k, \theta'), \tag{2.20}$$

where the network weights θ and θ' are used to parameterize the action value function. During training, initially, the agent takes actions more randomly to explore different states and stores the experiences as a tuple (current state, action taken, reward collected, next state) in the memory. When the network has enough experience, memory replay is invoked to train the target network. The experiences in the memory are randomly sampled to train the network. The process of training from experiences and sampling from the replay memory that stores the experiences is called experience replay. This reduces the correlation between the samples and therefore leads to efficient learning. To train our neural network, we use the loss function which is defined as the squared difference between the two sides of the Bellman equation and calculated as follows

$$L(\theta) = \mathbb{E}[(r + \gamma \max_{\mathbf{a}' \in \mathcal{A}} Q_k(s'_k, a'_k, \theta') - Q_k(s_k, a_k; \theta))^2]. \tag{2.21}$$

We use gradient descent to minimize the loss function [66] in (2.21). The number of neurons in the first and final layers is determined by the dimensions of the state space $|\mathcal{S}|$ and action space $|\mathcal{A}|$, respectively.

We consider the decaying ϵ-greedy exploration method to maintain a balance between exploration and exploitation. At a given epoch, the agent selects a random action with probability ϵ and opts for the best action where the Q-value is the highest with probability $1 - \epsilon$. Therefore, the probability of selecting action a_k in state s_k is defined as

$$\pi_k(s_k, a_k) = \begin{cases} \epsilon/(|\mathcal{A}| - 1), & otherwise \end{cases} \tag{2.22}$$

To fill the experience replay buffer, the algorithm tends to explore more at the beginning of the training. This makes sure the agent learns about the variation in the environment by starting with a random policy. We let $\epsilon = 1$ at the start and let it decay with each learning episode, and then finally set it at a small value $\epsilon = 0.01$. This means more exploitation after training for some episodes in which actions follow the policy.

The learning rate controls the change in the model each time we update the model weights. We implement a decaying learning rate model to balance between the accelerated training speed and the convergence to the optimal set of weights as well as avoiding the unstable training process. A too small value of the learning rate will lead to a long training process while a too large value may lead to convergence to a sub-optimal set of weights too fast. Therefore, the learning rate is an important hyper-parameter to configure for the neural network. The decaying learning rate is given as

$$\alpha(\Gamma) = \frac{\alpha_0}{(1 + \eta\Gamma)}, \tag{2.23}$$

where α_0 is the initial learning rate, Γ is the episode number of the training and η is the constant parameter for the decaying rate.

Algorithm 2 DQN Based Service Availability Oriented Mobility Management Algorithm

$\Gamma \leftarrow$ Training Episodes;
Hyper-parameters: learning rate $\alpha \in (0, 1]$, discount rate $\gamma \in [0, 1)$, ϵ-greedy rate $\epsilon \in (0, 1]$
Initialize: replay buffer memory $\mathcal{D}$, mini-batch size $\mathcal{M}$, and DQN parameters (θ, θ') for main and target networks.
$\mathcal{S}, \mathcal{A}$: State and Action space of the DQN agent
for each episode $\leftarrow 1$ to Γ **do**
  Update $\alpha(\Gamma)$ from (2.23)
  UAV with state s_1 initialized with random action a_1
  for $t = 1, 2, \cdots$ **do**
    if $p_\epsilon \leq \epsilon$ *//(p_ϵ is random probability)* **then**
      Select a random action $a_t \in \mathcal{A}$
    else
      Select $a_t = \arg\max_{a \in \mathcal{A}} Q(s_t, a, \theta)$
    end if
    Return $\Phi(l, b, t), \quad \forall l, b;$
    The UAV observes s_{t+1}
    Collects the reward r_t from (2.19)
    Stores the tuple (s_t, a_t, r_t, s_{t+1})
    Samples the random mini-batch of transitions (s_i, a_i, r_i, s'_i) from D;
    for each $i \in \mathcal{M}$ **do**
      $Q_i(s_i, a_i; \theta) = r + \gamma \max_{\mathbf{a}' \in \mathcal{A}} Q_i(s'_i, a'_i, \theta')$
      Compute Loss and perform gradient descent for $Q(s, a; \theta)$
      Update the target network parameters $\theta' = \theta$
    end for
  end for
end for=0

2.4 Results and Discussion

In this section, we compare the performance of the proposed schemes with a benchmark scheme. To have a fair comparison of the two approaches, all the system settings and parameters that are common in these schemes must be kept the same. We investigate the performance of our SA-MRO and DQN-powered learning solution and compared their results with the following benchmark scheme:

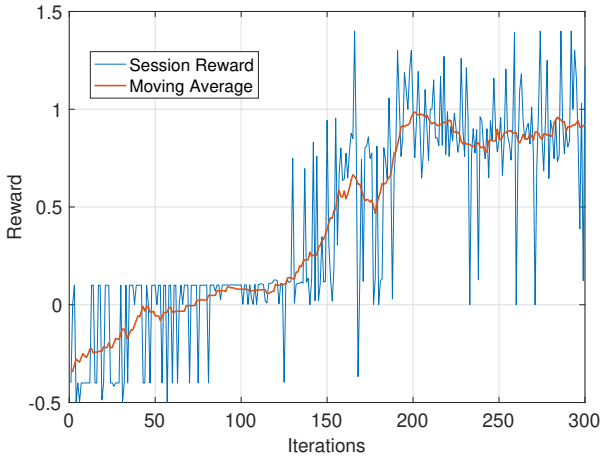

Figure 2.3: Numerical results showing session and average rewards against training iteration for the convergence of the proposed learning based algorithm (Reprinted from [1], ©2024 IEEE, reused with permission).

2.4.1 Simulation Environment

For the simulation setup, we consider 3 km $\times$ 3 km areas with 8 ground BSs uniformly distributed. The Algorithm 1, Algorithm 2, and the benchmark scheme are implemented in Python. We assume that each UAV is flying at a constant altitude of h and a speed of v. Our learning based solution targets that (i) for each time frame, i.e., 10 TTIs, each UAV should be associated with the serving BS having the best channel quality; (ii) at each TTI, UAV should be connected to only one BS; and (iii) for decreasing the buffer queue data, the UAV should connect to the best channel BS. We perform the learning with multiple UAV flights and then save our model for testing. The learning model selects the velocity and altitude of the UAV randomly thus making the trained model applicable to all the velocities and altitudes. The other system parameters used are provided in Table 2.2.

2.4.2 Behavior Analysis of the Proposed Algorithms

In this section, we present the results of the convergence of the learning based algorithm and the behaviour analysis in the time domain of the proposed SA-MRO algorithms.

Convergence of the learning based algorithm: To observe if our system is converging with training, we investigate the change in average session reward with respect to the number of iterations, which is shown in Fig. 2.3. The reward is given by (2.19), where all the KPIs are normalized and the sum of the weights (α_{r}, α_{d}, and α_{h}) is equal to one. This is done for two reasons: 1) the normalization

makes sure that all the KPIs contribute to the reward equally, i.e., none of the KPIs dominates the reward function and 2) the sum of the weights equal to one makes sure that the neural network takes the decisions based on the relative importance of the KPIs. In Fig. 2.3, we see the reward initially being negative as the system takes random actions which leads to multiple handovers, and the agent is penalized by the negative reward. As the training progresses and the agent learns from the previous actions, the rewards start to improve and the agent converges to a desired policy. Since we always have some random action as ϵ never goes to zero but is very small, which means the random actions lead to some fluctuations we can see in Fig. 2.3.

Analysis on Policy Design: It is not enough that the DQN algorithm converges, it is also important to know to which policy the algorithm has converged. To understand the converged policy, we observe the change in service availability and percentage of handovers as the agent trains in Fig.2.4. Different policies in the RL mean how the coefficients in the reward function are assigned and the agent converges to that policy, i.e., at which state which action is the best as per that policy. In our case, we want the agent to take action in such a way that a high service availability is maintained with few handovers. Fig.2.4 captures the progressive shifts in service availability and the percentage of handovers as the agent undergoes training using Algorithm 2. As can be observed from Fig. 2.4, after the first 150 iterations, the system starts to learn, and the service availability is increased by 90% while the number of handovers is reduced by 50%. This shows that the system learns according to the desired policy. After a higher number of iterations, the system becomes more stable, and we observe that the service availability remains constant with handovers below 10% as compared to the initial number of handovers.

Behavior Analysis of SA-MRO: In our proposed SA-MRO scheme, we dynamically adapt the parameters HOM and TTT according to the buffer queue state information of the UAV as explained in Algorithm 1. Fig. 2.5 shows the sensitivity of handover parameter HOM Ψ in response to variations in the buffer queue size $q(t)$. Notably, when the data in the buffer is low (falls below a predefined

Table 2.2: Simulation Parameters

Parameters	**Values**
Service area	3×3 Km^2
Available RRBs for UAV (per TTI)	Random, up to 4×180 KHz
BSs antenna height, carrier frequency	25 m, 2 GHz
Packet arrival rate and size at UAV	0.3 packet per sec; 2 Kbits
Handover control packet size	4×1 Kbits
$\Delta(\Psi)$, $\Delta(\Omega)$	0.5 dB, 10×TTIs [67]

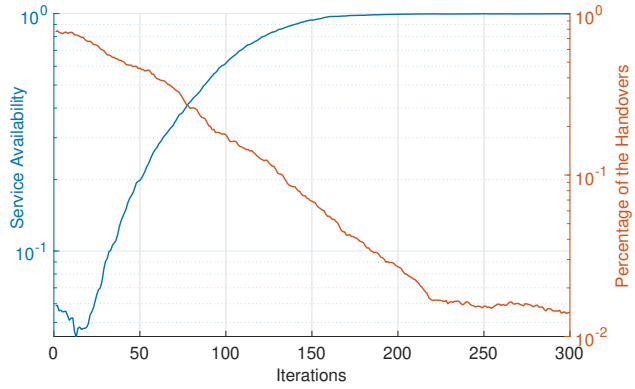

Figure 2.4: Numerical results showing the learned policy as the agent undergoes training using Algorithm 2 (Reprinted from [1], ©2024 IEEE, reused with permission).

threshold ($q_0 = 20$ kbits)), the algorithm increases the value of HOM Ψ till its maximum allowed value of 7 dB. The increased value of HOM will reduce the number of handovers, prompting the system to encourage the UAV to maintain its connection with the serving BS. Conversely, as the buffer queue size surpasses the threshold, the algorithm decreases the value of the parameter HOM Ψ, facilitating a faster handover to a stronger BS. This adaptive mechanism enhances data rate, expedites buffer data depletion, and improves overall service availability. Therefore, Algorithm 1 effectively minimizes unnecessary handovers while ensuring the buffer queue size remains below the stipulated threshold. To address challenges encountered during the initialization phase of parameter tuning, the system adopts a strategic approach. It initiates with the lowest possible HOM value, prioritizing the establishment of a robust connection with the strongest BS. Whether the system resets or a new user initiates data transmission, the HOM defaults to its lowest value by design. This approach ensures that the primary focus during these initial phases is on establishing and maintaining a reliable connection with the user.

2.4.3 Model based vs learning based handover management

The results for the outage probability, i.e., the probability that the queue size is greater than the threshold q_0 as defined in (2.15) are presented in this section. Fig. 2.6 shows the outage probability as a function of the UAV altitude for different approaches. The benchmark schemes with HOM = 7 dB and HOM = 2 dB have no interest in improving the UAV up-link communication service availability. They only care about keeping the connectivity with the network, and hence they are the first (HOM = 7 dB) and the second (HOM = 2 dB) most unreliable approaches. We consider the mobility of the UAV with velocities 30 m/s in Fig. 2.6(a), 40 m/s in Fig. 2.6(b) and 50 m/s in Fig. 2.6(c). In Fig. 2.6, the two cases of a fixed HOM considered are; a low HOM of 2 dB which favors more handovers and a high HOM

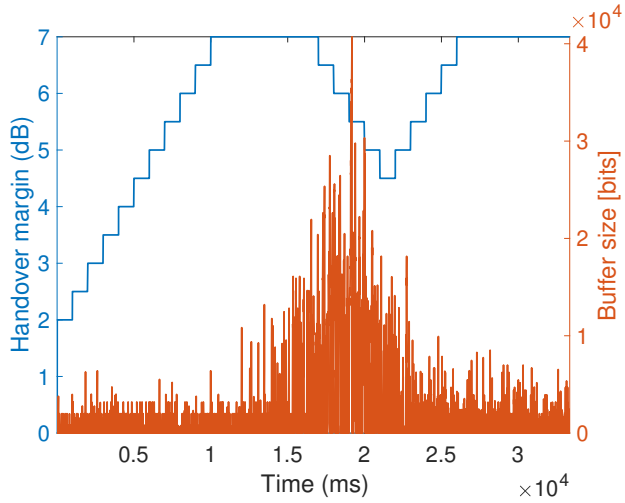

Figure 2.5: Numerical results showing the sensitivity of handover parameter HOM against the buffer queue size in time for the SA-MRO (Reprinted from [1], ©2024 IEEE, reused with permission).

of 7 dB margin which favors less handovers. The two HOMs provide us the two extreme cases in the benchmark scheme where we are only concerned about the connectivity of the mobile user. We observe in Fig. 2.6(a), the outage probability for the proposed learning based solution is less than 0.01 for all the altitudes and close to 0.01 for the proposed model based SA-MRO scheme. It indicates that both the proposed schemes care about service availability and force the system to take handover decisions in such a way as to keep the service availability high. We observe that the service availability improves as altitude increases. This is because, as the UAV altitude increases, the LoS increase as given in (3.1), making the channel condition better and thus increasing the data rate and emptying the buffer much faster. Also, as the speed of the UAV increases in Fig. 2.6(b) and Fig. 2.6(c), the difference between the SA-MRO and learning based approaches increases indicating that the model based approach is not suitable for highly mobile users. The learning based solution can maintain a low outage probability (< 0.01) in all the cases.

In Fig. 2.7, we observe the normalized number of handovers with respect to the UAV altitude, normalized to the scheme having maximum handovers. Our first observation is that as the altitude of the UAV increases, the number of handovers increases in all approaches. This is because, the number of BSs with which a UAV has LoS link increases as the altitude increases, also signal strength from the side lobes of the far-off BSs gives more opportunity for the handovers with those BSs. Secondly, the proposed learning based approach even with high service availability has only about 25% of handovers as compared to the benchmark scheme having a fixed HOM of 2 dB. This shows that the proposed learning based solution can

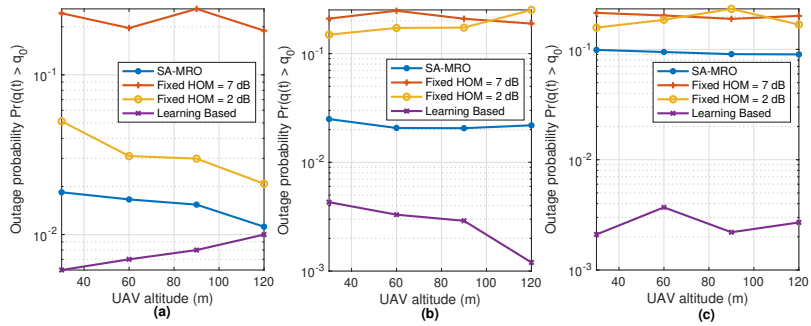

Figure 2.6: Numerical results for comparison of outage probability $Pr(q(t) \geq q_0)$ vs. UAV altitude (meters) for different UAV velocities. (a) $v = 30$ m/s (b) $v = 40$ m/s (c) $v = 50$ m/s (Reprinted from [1], ©2024 IEEE, reused with permission).

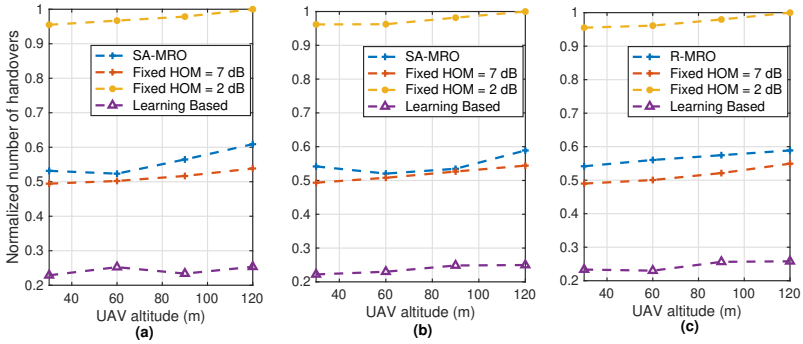

Figure 2.7: Numerical results for comparison of normalized number of handovers vs. UAV altitude (meters) for different UAV velocities. (a) $v = 30$ m/s (b) $v = 40$ m/s (c) $v = 50$ m/s (Reprinted from [1], ©2024 IEEE, reused with permission).

reduce the unnecessary handover while maintaining the high service availability. The proposed model based scheme SA-MRO also performs very well as the number of handovers are close to the benchmark scheme having a fixed HOM of 7 dB, showing that it can reduce the number of handovers while maintaining good service availability. Comparing the results from Fig. 2.6 and Fig. 2.7, we observe that, for the velocity of 30 m/s (Fig. 2.6(a), 2.7(a)), the SA-MRO achieves high service availability with less number of handovers but as the speed increases (Fig. 2.6(c), 2.7(c)), even though the number of handovers is less but the service availability also decreases. The learning based approach is not affected much by the velocity of the UAV and can achieve high service availability with a low number of handovers.

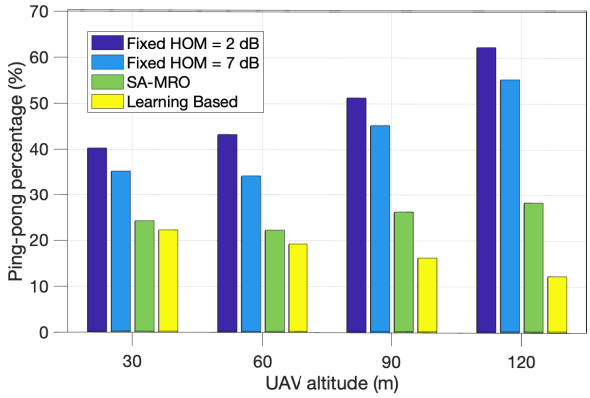

Figure 2.8: Numerical results showing ping-pong percentage vs. UAV altitude (m), for different mobility management schemes, with velocity $v = 30$ (m/s) (Reprinted from [1], ©2024 IEEE, reused with permission).

2.4.4 Ping-Pong effect

We also investigate the performance of the proposed algorithms in terms of the ping-pong rate. The numerical results for the comparison of the ping-pong handover percentage between learning based approach, SA-MRO, and the existing handover approach for different UAV altitudes are shown in Fig. 2.8. It can be observed that the learning based approach and the SA-MRO reduce the ping-pong effect at all the UAV altitudes. At higher altitudes, the proposed approaches can achieve a very low ping-pong percentage compared to the fixed HOM, resulting in up to 7 times reduction.

In Fig. 2.9, we show the numerical results for the distribution of the UAV queue lengths for the UAV up-link communication for all the approaches. Since the benchmark approach does not care about the data in the queue, we observe that for fixed HOM of 7 dB, there are long tails that can lead to extreme cases of latency and can affect the up-link communication quality of service severely. The proposed approaches control these extreme tails thus making sure that the UAV does not experience extreme delays.

2.5 Conclusion

In this chapter, two innovative approaches for managing the mobility of cellular-connected UAVs with a focus on service availability have been introduced. The initial solution employs a model-based strategy that utilizes the SA-MRO algorithm to adjust handover trigger parameters. The objective of the SA-MRO algorithm is to enhance service availability while minimizing the frequency of handovers. This

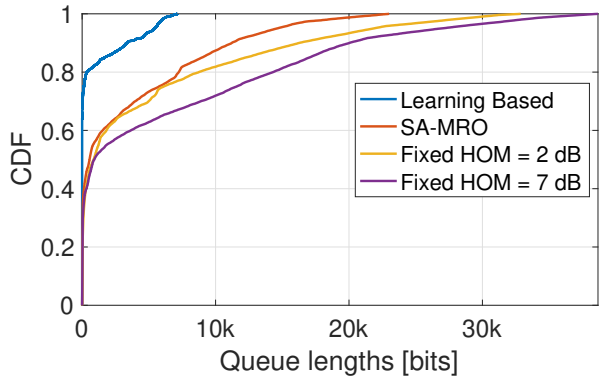

Figure 2.9: Numerical results of the distribution of the queue lengths exceeding q_0, showing impact of handover decision on the queue lengths (Reprinted from [1], ©2024 IEEE, reused with permission).

algorithm periodically optimizes the handover parameters (HOM and TTT) based on the buffer queue state information of the UAV. The second approach utilizes a learning-based method, employing a model-free DQN algorithm to determine BS association and radio resource allocation for cellular-connected UAVs. The DQN algorithm also aims to improve service availability while reducing queuing delay and the number of handovers. A multi-layer deep neural network is trained to approximate the Q-function for state-action pairs. Dynamic system-level simulations, implemented in Python using the 3GPP-defined urban micro scenario, are conducted to compare the performance of the proposed algorithms. Both solutions are designed to be implemented on the network side in the Radio Access Network (RAN) intelligent controller.

The findings indicate that, in most cases, traditional mobility management with fixed handover parameters leads to a degradation in service availability, characterized by an outage probability exceeding 0.1 and a high number of handovers. In contrast, the two proposed algorithms enhance service availability, with the outage probability for the learning-based algorithm falling below 0.01 and approximately 25% of handovers. For the SA-MRO algorithm, the outage probability ranges from 0.1 to 0.01, with about 50% of handovers. Both proposed solutions, compared to legacy mobility management with fixed handover parameters, reduce the ping-pong percentage by over 40%. Additionally, the analysis demonstrates that making handover decisions based on the queue state information of the UAV helps avoid cases of extreme delay tails.

Chapter 3

Localizability of Unmanned Aerial Vehicles

The applications of the unmanned aerial vehicles (UAVs) include rescue, monitoring, and transportation require beyond visual line of sight (BVLOS) operation. One enabler of the BVLOS operations is the precise localization of UAVs [68,69]. Different solutions are being investigated to obtain the location information of UAVs for their navigation and safe operation. A widely adopted solution is to use Global Positioning System (GPS) based localization. However, in the case of UAVs that have 3-dimensional (3D) mobility, GPS accuracy performance is still not satisfactory due to altitude-dependent shadowing. Many solutions including using ultraviolet light-emitting diodes on UAVs [33], using a radar-based localization system [35], and using sensors on the ground [70] are being investigated for the localization of the UAV in the sky.

An alternative approach is to utilize cellular networks so that the UAV can exploit the RF signals from the neighboring BSs to localize itself [43]. This approach is highly promising due to the current effort to integrate UAVs into cellular networks, i.e., cellular-connected UAVs [71]. They coexist with terrestrial mobile users while maintaining a certain level of quality of service [3, 72]. Furthermore, cellular networks with ubiquitous coverage provide the backbone for the UAVs to transmit mission-related data and also a certain level of reliability for the command and control signaling. Hence, exploitation of the ground infrastructure for the localization of UAVs presents opportunities and overcomes the challenges of extra hardware deployment.

The localization process is divided in two steps. The first is to obtain the localization signals from a set of sources to the target. The second is to use those signals to estimate the location of the target device. Mostly, calculating or improving the accuracy of estimating the location of the device is targeted [73]. During estimation, it is assumed to receive a set of strong signals from the required number of sources. This is not true in general, and more importantly not true in cellular net-

works where interference can play a major role. To analyze if a received signal can be utilized for localization, signal to interference plus noise ratio (SINR) is a good metric to use. We focus on this first step of the localization process, and utilize the term B-localizability as the probability that at least B number of BSs in the network can successfully participate in the localization process [41, 43]. That is at least a B number of BSs have the SINR greater than the required threshold. Each localization method like received signal strength indicator (RSSI), time difference of arrival (TDOA), angle of arrival (AOA), and observed time difference of arrival (OTDOA) has its minimum required number of participating BSs. For instance, in the case of the TDOA based method, we need at least three localization signals from different sources to locate a target device. The main contributions of the study can be summarized as follows:

- We propose an analytical framework to analyze the UAV localizability, i.e, the ability to be localizable. Our interest is the downlink localization for cellular-connected UAVs. Impact of the UAV altitude, the number of participating BSs and network coordination on the localizability performance are studied in detail. We investigate the effect of environment for three different scenarios: urban micro (UMi), urban macro (UMa), and rural macro (RMa).

- We derive the cumulative distribution functions (CDFs) and probability density functions (PDFs) of the path loss, interference and received SINR at the target UAV. This includes undertaking the A2G channel characteristics into consideration like effect of the UAV altitude on LOS and non-line of sight (NLOS) channel conditions.

- An optimization problem is formulated to find the altitude that maximizes the localizability. We performed approximations to solve the problem and obtain localizability performance.

- We provide insights toward the design parameters like processing gain requirement and network coordination for enhancing the signal strength for the localizability of UAVs.

3.1 System Model

We model the network as a two-tier cellular network with hexagonal tessellation for analytical tractability, which is a common assumption for 5G and beyond networks [74]. The two-layer hexagonal tessellation comprises 19 BSs (denoted as $T = 19$), the UAV to be localized (also referred to as target UAV) is assumed to be within the boundaries of the center cell at an altitude denoted by h_{UT}, depicted in Fig. 3.1. The dashed brown arrows shown in Fig. 3.1 represent the localization signals received by the target UAV from the BSs participating in the localization process. Distance relations between the UAV and one of the participating BSs are shown

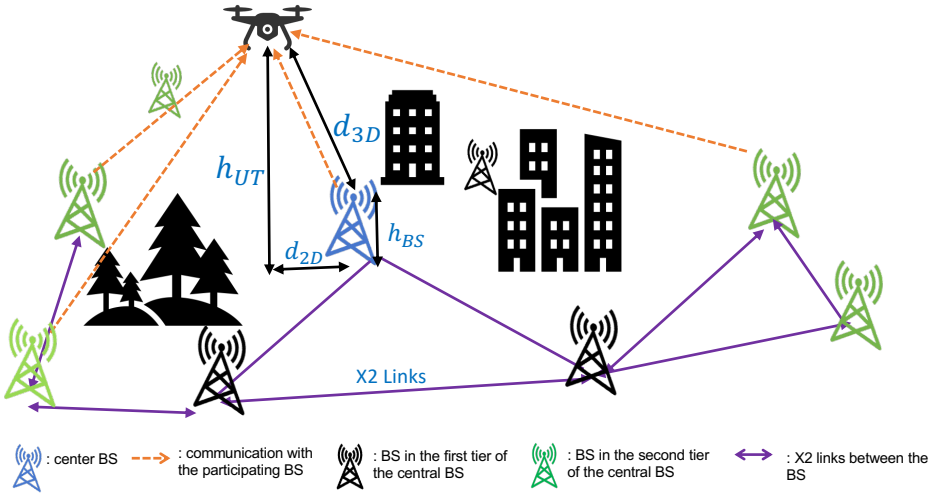

Figure 3.1: System model for cellular localizability, localization signals and distance relations (Reprinted from [2], ©2023 Elsevier, reused with permission).

with the black solid arrows in Fig. 3.1. Key notations to explain the system model are provided in Table 3.1.

We consider the downlink positioning, which involves the transmission of localization signals from the BSs to the UAV [75]. We also assume universal frequency reuse on the localization signals. The adjacent BSs share control information with each other via the high-speed backhaul links e.g., X2 interface shown in Fig. 3.1. The X2 links enable synchronization and coordination among the BSs [76]. We consider the three 3GPP-defined scenarios for the UAVs [3]; UMi-AV (urban micro with aerial vehicles), UMa-AV (urban macro with aerial vehicles), and RMa-AV (rural macro with aerial vehicles).

For any localization method to work, the target UAV must receive localization signals from multiple sources with an SINR value greater than a specific threshold. The number of sources and the threshold depend on the localization method implemented. For example, in the timing based localization, the estimated time difference translates into circles around the BS, and the intersection of these circles provides the location of the target UAV. For better accuracy, more BSs should participate in the multilateration procedure. The minimum required number of participating BSs changes for different methods. For instance, in the case of AOA and TDOA, the minimum requirements for the number of participating BSs are two and four, respectively [77].

Under the same modulation and coding scheme, interference from the other BSs acts as one of the major hindrances in obtaining localization signals from the required number of participating BSs. Thus, making the SINR as the most suitable metric to capture the effectiveness of any localization signal. Furthermore, after

Table 3.1: Key Notations Used.

Notation	Description
h_{UT}, h_{BS}	Altitude of the UAV, base station height
d_i	3D distance between the UAV and i-th participating BS
d_k	3D distance between the UAV and k-th non-participating BS
P_t	Transmitted power from the BS
ζ	Independent shadowing effect
σ^2	Variance of the additive white Gaussian noise
PL_m	Path loss between BS and the UAV, $m \in \{LoS, NLoS\}$
T	Total number of BSs in the network
$\mathcal{T}$	Set of BSs in the network
B	Number of BSs taking part in the localization of the UAVs
f_c	Carrier frequency used
$\mathcal{I}_1$	Interference from BSs participating in localization
$\mathcal{I}_2$	Interference from BSs not taking part in localization
$\mathcal{I}$	Total cumulative interference to the localization of the UAV
α	SINR threshold before the processing gain
β	SINR threshold after the processing gain
γ	Processing gain required
p	Activity factor modeling the coordination among the B participating BSs
q	Activity factor modeling the network traffic load from $(T - B)$ non participating BSs
r_k	Indicator variable, equal to one with probability p, and equal to zero with the probability $(1 - p)$, for the k-th BSs
s_j	Indicator variable, equal to one with probability q, and equal to zero with the probability $(1 - q)$, for the j-th BSs
P^z	Probability of LoS ($z = LoS$) and NLoS ($z = NLoS$)
P_B	Probability that B BSs have SINR greater than threshold

the UAVs have processed the localization signals, they transmit their location information with payload data. We make the assumption of seamless synchronization among the participating BSs. This synchronization is attained through packet-based time alignment, commonly implemented using the Precision Time Protocol (PTP), which is specified as IEEE 1588 [78].

3.1.1 Channel Model

In this paper, we adopt the 3GPP channel model proposed in [3] for cellular-connected UAVs flying below 120 m. The channel model depends on the probability of LoS, P^{LoS}, which is defined as below:

$$P^{LoS} = \begin{cases} 1, & d_{2D} \leq d^1 \\ \frac{d^1}{d_{2D}} + \exp\left(\frac{-d_{2D}}{p_1}\right)\left(1 - \frac{d^1}{d_{2D}}\right), & d_{2D} > d^1 \end{cases}, \tag{3.1}$$

where d_{2D} is the distance between the BS and the UAV projected on the ground plane, h_{UT} is the altitude of the UAV as seen in Fig. 3.1. h_{UT} can be greater or smaller than the height of the BS, h_{BS}. The parameters p_1 and d^1 for three scenarios are given in Table 3.2.

The path loss PL_m, where $m \in \{\text{LoS}, \text{NLoS}\}$ for the LoS and NLoS link conditions, respectively, are calculated as follows [3]:

$$PL_{LoS} = 28.0 + 22\log_{10}(d_{3D}) + 20\log_{10}(f_c), \tag{3.2}$$

$$PL_{NLoS} = -17.5 + (46 - 7\log_{10}(h_{UT}))\log_{10}(d_{3D}) + 20\log_{10}(\frac{40\pi f_c}{3}), \tag{3.3}$$

where d_{3D} is the 3D distance between the BS and the UAV, and f_c is the carrier frequency in GHz.

We incorporate shadowing effects, where signal variations are modeled by a Gaussian distributed random variable ζ with a standard deviation that varies with height [3], described as $4.64\exp(-0.0066h_{UT})$ (for LoS), 6 dB (NLoS). However, the effects of small-scale fading are neglected, as they tend to be smoothed out when considering the average signal strength. This average incorporates broader temporal factors like path loss and shadowing and is consistent with the current models for evaluating cellular localization performance [79, 80].

3.1.2 Antenna Gain

In our system model, we consider a single omnidirectional antenna with unitary gain for the UAV. For the ground BSs, we assume a vertical N-element uniform linear array (ULA), where each element is omnidirectional in azimuth with a maximum gain of g_E^{max}. Directivity as a function of the zenith angle (ϕ) is given by the following [60]:

$$g_E(\phi) = g_E^{max} \sin^2(\phi), \tag{3.4}$$

where ϕ is the zenith angle between the ground BS and the UAV. Considering half-wavelength spacing between the adjacent antenna elements and a fixed down-tilt angle ϕ_t, the array factor of the ULA is calculated as

$$g_A(\phi) = \frac{\sin^2(N\pi(\cos\phi - \cos\phi_t)/2)}{N\sin^2(\pi(\cos\phi - \cos\phi_t)/2)}. \tag{3.5}$$

The overall antenna gain of BSs in linear scale is calculated as

$$g(\phi) = g_E(\phi) \times g_A(\phi). \tag{3.6}$$

Table 3.2: 3GPP Channel Model Parameters [3].

Scenario	p_1	d^1
UMi-AV	$233.98\log_{10}(h_{UT}) - 0.95$	$\max(294.05\log_{10}(h_{UT}) - 432.94, 18)$
UMa-AV	$4300\log_{10}(h_{UT}) - 3800$	$\max(460\log_{10}(h_{UT}) - 700, 18)$
RMa-AV	$\max(15021\log_{10}(h_{UT}) - 16053, 1000)$	$\max(1350.8\log_{10}(h_{UT}) - 1602, 18)$

3.1.3 SINR Calculation

Based on the above channel models, the received SINR at the UAV at altitude (h_{UT}) from an ith ($i \in \mathcal{T}$) BS, which is at a 3D distance of $d_{3D} = d_i$ is calculated as

$$SINR_i = \frac{P_r(h_{UT}, d_i)}{\mathcal{I} + \sigma^2}, \tag{3.7}$$

where $P_r(h_{UT}, d_i)$ is the received power and is given as

$$P_r(h_{UT}, d_i) = P_t g_i(\phi) \zeta_i P L_m^{-1}(h_{UT}, d_i), \tag{3.8}$$

where P_t is the transmitted power from the ith BS to the UAV and is assumed to be same for all the BSs, $g_i(\phi)$ is the antenna gain, ζ_i denotes the independent shadowing affecting the signal strength. The cumulative interference from the concurrently transmitting BSs excluding the ith BS is denoted by $\mathcal{I}$ and is calculated as

$$\mathcal{I} = \sum_{k \in \mathcal{T} \text{ and } k \neq i} P_t g_k(\phi) \zeta_k P L_m^{-1}(h_{UT}, d_k), \tag{3.9}$$

where d_k is the 3D distance between the UAV and the kth BS ($k \in \mathcal{T}$ and $k \neq i$), which are transmitting at the same time. Among the $|\mathcal{T}| = T$ BSs, B number of BSs ($B \leq T$) with the strongest time average received signal strength participate in the localization process. However, their participation is successful only if they have SINR greater than a given threshold.

A processing gain γ is considered to enhance the localizability signal strength by integrating the incoming signals in time. Therefore, we have two SINR definitions at the receiver: pre-processing SINR, which is the SINR before any processing gain, and post-processing SINR after applying the gain. The pre-processing SINR provided in (3.7) is given without the gain providing an improvement on the localization signal strength to meet the requirements.

It is also important to note here that the 5G opens new dimensions to improve the localization performance thanks to New Radio (NR) framework [80]. It proposes new capabilities such as downlink positioning reference signal (PRS) with different numerology and frequency options such as frequencies below 6 GHz and above 24 GHz. BSs can utilize different PRS sequences to reduce mutual interference. These sequences can follow different comb structures that use certain subcarriers in designated symbols [81].

In case of the UAV, as the altitude increases, the probability of LoS condition with ground BSs increases resulting in better reception of useful signals from the intended BS. However, it also leads to a higher level of interference from the unintended BSs. To avoid interference, the B participating BSs attempt to coordinate and avoid allocating the same radio resources. However, perfect coordination among all B BSs is not always possible. As a result, they simultaneously transmit their localization signals on the same radio resources with a probability p. The parameter p encapsulates the effectiveness of X2 link performance in facilitating

coordination among the participating BSs. A value of $p = 0$ indicates perfect coordination achieved through X2 links, resulting in no interference, while $p = 1$ signifies the absence of coordination via X2 links. Meanwhile, due to network load, each of the remaining $(T - B)$ BSs may also transmit simultaneously using the same radio resources with probability q. To account for coordination among the participating BSs and the traffic demands in the non-participating BSs, we introduce two independent random variables: r_k for the participating BSs and s_j for the non-participating BSs. To capture participating and non-participating BSs in our analysis, the SINR calculated in (3.7) can be reformulated as:

$$SINR_i(B) = \frac{P_t g_i(\phi)\zeta_i PL_m^{-1}(h_{UT}, d_i)}{\mathcal{I}_1 + \mathcal{I}_2 + \sigma^2}, \tag{3.10}$$

where $\mathcal{I}_1$ represents the cumulative interference from the participating BSs and $\mathcal{I}_2$ represents the cumulative interference from the non-participating BSs. Their mathematical definitions are given as follows:

$$\mathcal{I}_1 = \sum_{k=1 \; and \; k \neq i}^{B} r_k P_r(h_{UT}, d_k) = \sum_{k=1 \; and \; k \neq i}^{B} r_k P_t g_k(\phi)\zeta_k PL_m^{-1}(h_{UT}, d_k), \tag{3.11}$$

$$\mathcal{I}_2 = \begin{cases} \sum_{j=1+B}^{T} s_j P_r(h_{UT}, d_j) = \sum_{j=1+B}^{T} s_j P_t g_j(\phi)\zeta_j PL_m^{-1}(h_{UT}, d_j), & \text{if B} < \text{T} \\ 0, & \text{if B} = \text{T} \end{cases}, \tag{3.12}$$

where r_k and s_j follow Bernoulli distribution. r_k and s_j being equal to one with probability p and q, respectively, and equal to zero with the probability $(1-p)$ and $(1-q)$, respectively. The activity parameters associated with participating and non-participating BSs make the $SINR_i$ in (3.10) as a function of B.

3.2 Theoretical Analysis of Localizability Performance

In this section, we develop a theoretical framework to analyze the localizability performance of a target UAV with the help of cellular networks. We first derive the B-localizability as the function of the received SINR and the number of participating BS B. The received SINR dependents on the received power, cumulative interference and noise. To obtain the distribution of the received power, we need to calculate the distribution of the distances and path loss involved. These steps are provided in the sequel.

3.2.1 Base Stations Participating in the Localization

Let us define a random variable Ψ as the maximum number of BSs successfully participating in the localization process. Given our system model, the definition of

Ψ is given as follows:

$$\Psi = \underset{B\in\mathcal{T} \text{ and } B\leq T}{\arg\max} \; B \times \prod_{i=1}^{B} \mathbb{1}\left(SINR_i(B) \geq \alpha\right), \tag{3.13}$$

where B is the number of BSs participating in the localization and having the strongest signal at the UAV, and SINR is given as in (3.10). $\mathbb{1}(\theta)$ is the indicator function which is equal to 1 if θ is true and equal to 0 if θ is false. Hence, Ψ will be equal to B when all the signals from the B BSs have an SINR value greater than the threshold.

We define B-localizability as the probability that at least B BSs successfully participate in the localization procedure [41]. B-localizability, P_B, is defined as:

$$P_B = \; Pr(\Psi \geq B) = 1 \; - \; F_\Psi(B), \tag{3.14}$$

where $F_\Psi(B)$ is the CDF of Ψ and is defined as:

$$\begin{aligned} F_\Psi(B) &= \; Pr(\Psi < B) = 1 \; - \; Pr(\Psi \geq B) \\ &= 1 - Pr\Bigg(\big(\prod_{i=1}^{B} \mathbb{1}\left(SINR_i(B) \geq \alpha\right) \big) \; = \; 1 \Bigg). \end{aligned} \tag{3.15}$$

The B-localizability metric can also be viewed as a coverage metric that quantifies the probability of receiving decodable localization signals from B BSs at the receiver. For instance, in the case of the TDOA localization scheme that requires at least four decodable signals ($B = 4$) for unambiguous localization, P_4 represents the probability of achieving this criterion. A value of $P_4 = 0.99$ indicates that the target UAV may receive at least four decodable signals with a probability of 99%.

The distribution of B-localizability in (3.15) depends on SINR distribution at the target UAV from participating BSs. Hence, we statistically characterize each component to calculate SINR defined in (3.10) in the following subsections.

3.2.2 2D Distance and Altitude Distribution

The received power and interference at the target UAV are influenced by the distance between the BSs and the UAV. Therefore, to determine the SINR distribution at the target UAV, we first need to calculate the distance distribution between the BSs and the UAV's projection point on the ground (i.e., 2D distance). Since the target UAV is located randomly in the central hexagon cell, it will have two random 2D distances associated with it, which will depend on the point of reference used for their calculation. Specifically, the first random distance is the distance between the random location of the target UAV and the central BS (or the center of the hexagon as the reference point), denoted as θ_x in Fig. 3.2(a). The second random distance is the distance between the random location of the target UAV in the central hexagon cell and any of the neighboring BS (used as the reference point), denoted as θ_y in

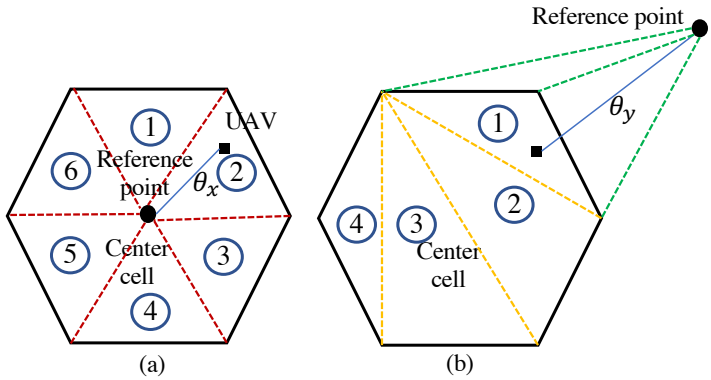

Figure 3.2: The random 2D distance between the UAV and the reference BSs, where the UAV is distributed randomly in the center cell. (a) θ_x is the 2D distance between a random point of the UAV within a cell and the BS at the center cell. (b) θ_y is the 2D distance between a random point of the UAV within a cell and the BS at a neighboring cell (Reprinted from [2], ©2023 Elsevier, reused with permission).

Fig. 3.2(b). Therefore, the first step is to determine the distributions of these two random distances: 1) the distance (θ_x) from a reference point inside the hexagon to a random point within the hexagon, and 2) the distance (θ_y) from a reference point outside the hexagon to a random point inside the hexagon.

Let $F_{\theta_x}(r)$ and $F_{\theta_y}(r)$ represent the CDF of θ_x and θ_y, respectively. To obtain the distribution of the random distances θ_x and θ_y, we adopt an approach similar to that presented in [82]. This approach involves the use of decomposition and recursion techniques to calculate the distance distribution in a polygon. Specifically, we use the known distance distributions from a vertex of an arbitrary triangle to a random point inside, to compute the distribution of random distances from an arbitrary reference point (inside or outside) to any polygon.

To implement this approach, we first triangulate (i.e., divide into triangles) the hexagonal cell with respect to the reference points. For calculating $F_{\theta_x}(r)$, the reference point is inside and at the center of the central hexagonal cell. Thus, we triangulate the cell into six triangles with respect to the center, as depicted in Fig. 3.2(a). Similarly, for calculating $F_{\theta_y}(r)$, the reference point is outside of the central hexagonal cell. Hence, we triangulate the cell into four non-overlapping triangles with respect to one of the vertex of the hexagon, as shown in Fig. 3.2(b).

Overall, this triangulation and decomposition approach allows us to obtain the distance distribution for a given reference point and polygon. Once we know the distribution of distances within each triangle, we can use probabilistic summation to compute the final distance distribution. Specifically, the CDF of the distance distributions $F_{\theta_x}(r)$ will be given by a probabilistic sum of the CDF of the distance distribution in each of the six triangles. Let $F_{\theta}^{\kappa}(r)$ represent the CDF of the distance distribution from a vertex to a randomly chosen point within a given triangle (κ),

such as triangle ② illustrated in Fig. 3.2(a). To ascertain the distance distribution from the vertex to a randomly selected point within the triangle (κ), we initiate the process by drawing a circle centered at the said vertex. In this setup, the radius of the circle, denoted as θ_x, corresponds directly to the distance between the vertex and the random point situated within the triangle (κ). The probability that this distance measures less than θ_x, essentially the CDF (F_θ^κ), is equal to the area of the intersection between the circle and triangle (κ) divided by total area of the triangle (κ), denoted as $\mathcal{A}_\kappa$ [82].

Subsequently, the CDF $F_{\theta_x}(r)$ for the distance distribution from the center to a randomly selected point within the polygon can be determined through probabilistic summation, given as:

$$F_{\theta_x}(r) = \sum_{\kappa=1}^{\Omega} \frac{\mathcal{A}_\kappa}{\mathcal{A}} F_\theta^\kappa(r), \tag{3.16}$$

where Ω is the number of triangles formed in the polygon with BS as the reference. $\mathcal{A}_\kappa$ is the area of the κth triangle, where $\mathcal{A}$ is the area of the cell. In the case of the hexagon where the triangulation takes place at the center, Ω is equal to six, which is seen in Fig. 3.2(a).

The CDF of the distance distribution F_{θ_y} is similar to $F_{\theta_x}(r)$ given in (3.16), but with one key difference: $F_\theta^\kappa(r)$ is the CDF of the distance distribution from a point outside of the triangle to a random point located in the κth triangle (e.g., triangle ① in Fig. 3.2(b)), which is provided in [82]. In Fig. 3.2(b), the reference point (in this case, the BS) is situated outside the center cell, the cell gets divided into four triangles with respect to one of its vertex. The CDF of the distance distribution F_{θ_y} will be given as the probabilistic summation of distance distributions for all four triangles in the central cell as in (3.16).

The other distance distribution for UAVs is for the altitude of the UAV. We assume a uniform distribution with a CDF of $F_H(h)$ within the limits between 20 m and 120 m.

3.2.3 Statistical Characterization of Path Loss and Received Power

Characterization of the path loss as the CDF at a certain altitude of h_{UT} is provided in the following due to its dependence on LoS probability:

$$F_{PL}(d) = \sum_{z \in \{LoS, NLoS\}} P^z F_{PL,z}(d), \tag{3.17}$$

where $F_{PL,LoS}(d)$ and $F_{PL,NLoS}(d)$ are derived as follows:

$$\begin{aligned} F_{PL,LoS}(d) &= Pr(PL_{LoS}(d_{3D}) \leq d) \\ &= Pr\left(\eta_{LoS}\left(\sqrt{d_{2D}^2 + h_{UT}^2}\right)^{a_{LoS}} \leq d\right) \\ &= Pr\left(d_{2D} \leq \sqrt{(d/\eta_{LoS})^{2/a_{LoS}} - h_{UT}^2}\right) \\ &= \sum_{\kappa=1}^{\Omega} \frac{\theta_\kappa}{\theta} F_\theta^\kappa(\sqrt{(d/\eta_{LoS})^{2/a_{LoS}} - h_{UT}^2}), \end{aligned} \tag{3.18}$$

where we model the path loss for the LoS condition in (3.2) as $PL_{LoS} = \eta_{LoS} d_{3D}^{a_{LoS}}$, η is the attenuation constant and a is the path loss exponent. Similarly, in case of the NLoS, the distribution for the path loss can be calculated as:

$$F_{PL,NLoS}(d) = \sum_{\kappa=1}^{\Omega} \frac{\theta_\kappa}{\theta} F_\theta^\kappa(\sqrt{(d/\eta_{NLoS})^{2/a_{NLoS}} - h_{UT}^2}), \tag{3.19}$$

Let R be the received signal strength at the UAV from a BS which can be described as the difference between the transmitted power (P_t) and the path loss (PL). Then, the CDF $F_R(r)$ of the received power is calculated as:

$$\begin{aligned} F_R(r) = Pr(R \leq r) &= Pr((P_t - PL) \leq r), \\ &= Pr((P_t - r) \leq PL), \\ F_R(r) &= 1 - F_{PL}(P_t - r). \end{aligned} \tag{3.20}$$

The PDF $f_R(r)$ of the received power is $f_R(r) = F_R'(r)$

3.2.4 Statistical Characterization of Interference

As provided in (3.10), the interference to the UAV is due to both participating BSs ($\mathcal{I}_1$) and non-participating BSs ($\mathcal{I}_2$). Both interference components, $r_k P_r(h_{UT}, d_k)$ and $s_j P_r(h_{UT}, d_j)$ given in (3.11) and (3.12) respectively, are products of independent binary variables and the continuous received signal strength random variable. The independent binary variables are used to model the cooperation with the participating BSs and the traffic load in non-participating BSs. Let χ denote the discrete binary random variable r_k or s_j depending on the BS to be either participating or non-participating one, and R denote the continuous received signal strength random variable ($F_R(r)$ is already defined in (3.20)). Hence, to represent interference to the UAV from a single kth ($k \in [1, B]$) participating BS, we define a new random variable $I_{1,k} = \chi R$. The CDF of the $I_{1,k}$ will be then as follows:

$$\begin{aligned} F_{I_{1,k}}(i) = Pr(\chi R \leq i) &= Pr(\chi = 1)Pr(\chi R \leq i \mid \chi = 1) \\ &\quad + Pr(\chi = 0)Pr(\chi R \leq i \mid \chi = 0), \\ &= \begin{cases} pF_R(i) + (1-p), & \text{if } i > 0, \\ (1-p), & \text{if } i = 0, \end{cases} \end{aligned} \tag{3.21}$$

where $F_R(i)$ is defined in (3.20), p is the probability r_k being equal to 1. $F_{I_{1,k}}(i)$ provides the distribution of interference at the UAV from a single participating BS. For the distribution of the interference from a jth ($j \in [B+1, T]$) non-participating BS, $F_{I_{2,j}}$, is derived in same way as in (3.21) with final expression as:

$$F_{I_{2,j}}(i) = \begin{cases} qF_R(i) + (1-q), & \text{if } i > 0, \\ (1-q), & \text{if } i = 0, \end{cases} \tag{3.22}$$

Under given conditions, we can consider the interference from the BSs as independent. $F_{I_{1,k}}(i)$ and $F_{I_{2,j}}(i)$ show the individual interference distribution from a single random BS.

The cumulative distribution of the overall interference at the receiver is obtained by the convolution of the individual interference distributions as follows:

$$F_I(i) = F_{I_{1,1}}(i) \circledast ... F_{I_{1,B}}(i) \circledast F_{I_{2,B+1}}(i) \circledast ... F_{I_{2,T}}(i), \tag{3.23}$$

where $\circledast$ is the convolution operator. The PDF $f_I(i)$ of the cumulative interference is the calculated as $f_I(i) = F_I'(i)$.

3.2.5 Statistical Characterization of SINR

The received SINR defined in (3.7) is a function of the received power and the cumulative interference. For simplicity of notation, we denote the SINR by S, the received power by R, and the cumulative interference by I. The probability distribution of the received SINR can be derived using the probability distributions of the received power $f_R(r)$ and cumulative interference $f_I(i)$. For tractability, we consider the received power and the cumulative interference to be bounded between a minimum and a maximum value, i.e., $R \in [r_{min}, r_{max}]$, and $I \in [i_{min}, i_{max}]$.

Given the value of any two out of the three parameters, S, R, and I, the value of the third parameter can be calculated using (3.7). Let the SINR corresponding to received power R and cumulative interference I be denoted by $g_S(R, I)$. The received power corresponding to the SINR value S and cumulative interference I is denoted by $g_R(I, S)$ and cumulative interference corresponding to SINR value S and received power R is denoted by $g_I(R, S)$.

Assuming that the received power R and the cumulative interference I are independent, the largest value of the SINR would be achieved when the received power is maximum and the interference is minimum and is given as $g_S(r_{max}, i_{min})$. The lowest value of the SINR is achieved when the received power is minimum

and the interference is maximum and is given as $g_S(r_{min}, i_{max})$. Therefore, we can obtain the CDF of the SINR at the UAV by considering $g_S(r_{min}, i_{max}) \leq S \leq g_S(r_{max}, i_{min})$. This is calculated as follows:

$$Pr(S \leq \alpha) = \begin{cases} \int_{g_I(\alpha, r_{min})}^{i_{max}} \int_{r_{min}}^{g_R(\alpha,i)} f_R(r) f_I(i) d_r d_i, \\ \qquad if\ g_S(r_{min}, i_{max}) \leq \alpha \leq g_S(r_{min}, i_{min}); \\ \int_{i_{min}}^{i_{max}} \int_{r_{min}}^{g_R(\alpha,i)} f_R(r) f_I(i) d_r d_i, \\ \qquad if\ g_S(r_{min}, i_{min}) \leq \alpha \leq g_S(r_{max}, i_{max}); \\ 1 - \int_{i_{min}}^{g_I(\alpha, i_{max})} \int_{g_R(\alpha,i)}^{r_{max}} f_R(r) f_I(i) d_r d_i, \\ \qquad if\ g_S(r_{max}, i_{max}) \leq \alpha \leq g_S(r_{max}, i_{min}); \end{cases} \tag{3.24}$$

Since it is also possible to have $g_S(r_{max}, i_{max}) < g_S(r_{min}, i_{min})$, the CDF of the SINR can also be written as follows:

$$Pr(S \leq \alpha) = \begin{cases} \int_{g_I(\alpha, r_{min})}^{i_{max}} \int_{r_{min}}^{g_R(\alpha,i)} f_R(r) f_I(i) d_r d_i, \\ \qquad if\ g_S(r_{min}, i_{max}) \leq \alpha \leq g_S(r_{max}, i_{max}); \\ \int_{i_{min}}^{i_{max}} \int_{r_{min}}^{g_R(\alpha,i)} f_R(r) f_I(i) d_r d_i, \\ \qquad if\ g_S(r_{max}, i_{max}) \leq \alpha \leq g_S(r_{min}, i_{min}); \\ 1 - \int_{i_{min}}^{g_I(\alpha, i_{max})} \int_{g_R(\alpha,i)}^{r_{max}} f_R(r) f_I(i) d_r d_i, \\ \qquad if\ g_S(r_{min}, i_{min}) \leq \alpha \leq g_S(r_{max}, i_{min}). \end{cases} \tag{3.25}$$

3.2.6 Operational Altitudes for Maximum Localizability

Based on the previous discussion, it is evident that the localizability performance is directly linked to the received SINR at the UAV. Additionally, due to the impact of the UAV altitude on both the channel gain and the antenna gain, the received SINR at the UAV is a non-linear function of the altitude. Therefore, our objective is to determine the relationship between the localizability performance in terms of (P_B) and the UAV altitude. We can achieve this by formulating an optimization problem that seeks to identify the altitude that maximizes the localizability performance

(P_B) as follows:

$$\max_{h_{UT}} \sum_{i \in \mathcal{T}} \mathbb{1}(SINR_i \geq \alpha) \tag{3.26}$$

subject to:

(C1) $h_{UT} \leq h_{\max}$,

(C2) $h_{UT} \geq h_{\min}$,

where **(C1)** stands for the maximum allowed altitude for the UAV, and **(C2)** assures that a UAV is moving in the air above a certain altitude as per [3]. The objective function in (3.26) maximizes the number of BSs with SINR greater than the threshold α with respect to the altitude of the UAV. The objective function in our case depends on the distribution of the SINR at the UAV given in Section 3.2.5. Since the distribution does not have a closed-form expression, it is difficult to solve this optimization problem with conventional optimization methods. Therefore, we use a discrete brute force approach with Monte-Carlo simulations for obtaining the dependence of localizability probability on the altitude of the UAV. This approach is explained as follows.

We assume that there are UAVs distributed randomly in a plane in the center cell at discrete altitudes. We seek to maximize the numbers of UAVs which receive an SINR greater than some threshold from at least B number of BSs with respect to the altitude of the UAV. Thus, we find the optimal altitude that maximizes the localizability of UAVs. Let j denote the location in the center cell where the UAV is located, h ($h_{min} \leq h \leq h_{max}$) denotes the UAV altitude and i ($i \in \mathcal{T}$) denotes considered BS. Next, we present our optimization problem whose goal is to determine the altitude of each UAV which maximizes the localizability by the network as follows:

$$\underset{h_{min} \leq h_{UT} \leq h_{max}}{\arg\max} \quad (\varphi_h), \tag{3.27}$$

$$\varphi_h = \sum_j b_{j,h}, \ \forall h \tag{3.28}$$

$$b_{j,h} = 1, \text{if } \sum_i a_{i,j,h} \geq B, \ \forall j, h; \tag{3.29}$$

$$a_{i,j,h} = 1, \text{if } (SINR_{i,j,h} \geq \alpha), \ \forall i, j, h; \tag{3.30}$$

where $SINR_{i,j,h}$ is the received SINR at UAV j at altitude h from BS i. $a_{i,j,h} = 1$ in (3.30) means the SINR from the BSs i to the UAV j at altitude h is above a certain threshold α, $b_{j,h} = 1$ in (3.29) means that total number of BSs having SINR greater than the threshold (α) is at-least B. The φ_h in (3.28) means the number of the location at which the SINR constraint is satisfied for B number of BSs at different altitudes. The objective function in (3.27) gives us the UAV altitude h_{UT} which maximizes the total number of locations at which the SINR from at least B BSs is greater than the threshold.

Note that there is no guarantee that limited samples of the UAVs in (3.30) capture the distribution of the SINRs. In order to solve this problem, we used our analytical calculation and compare the simulation results obtained using the approach in (3.28)-(3.30) as shown in Fig. 3.3. Since the simulation results and the analytical results are overlapping, it shows that our approach captures the analytical evaluation.

3.3 Simulation Results and Discussion

We use Monte Carlo simulation and the snapshot model to analyze the localizability in Matlab. In our simulations, we performed 100,000 iterations with the target UAV randomly located in the center cell to obtain the localizability probability. We adopt the 3GPP channel model for the UAVs [3] in three different scenarios: UMi-AV, UMa-AV, and RMa-AV. The simulation parameters are given in Table 3.3.

Table 3.3: Parameters for numerical study.

Parameters	**UMi-AV**	**UMa-AV**	**RMa-AV**
Inter-site distances	200m	500m	1732m
BSs antenna height	10m	25m	35m
Carrier frequency	2 GHz	2 GHz	800 MHz
Bandwidth (B_w)	10 MHz		
Noise figure (NF)	9 dB		
Transmit power	46 dBm		
Maximum element gain (g_E^{max})	8 dBi		
Number of elements (N)	8		
Down-tilt angle (ϕ_t)	102°		
Variance	$4.64\exp(-0.0066h_{UT})$(for LoS), 6 dB(NLoS)		
Noise Power [dBm]	$10\log_{10}(400 \cdot 10^{-20}) + NF + 10\log_{10}(B_w)$ [83]		

3.3.1 B-Localizability Performance

In the case of 3D mobility of cellular-connected UAVs, it is hard to obtain an exact SINR distribution due to its dependency on air-to-ground channel characteristics with LoS conditions and changing shadowing variance with the UAV's altitude, and cooperation between participating and non-participating BSs. The SINR distribution provided in Section 3.2.5 is computationally intensive. Hence, to provide the analytical results, we use an approximate method. We use (3.16) to get the distance distribution of the UAV in the central cell of the network. The received power and the interference are obtained from (3.20)-(3.23), for different locations in the central cell. Hence, to have approximate results for the analytical derivations that we present in Section 3.2, we use empirical CDFs for resulting SINRs. According to these CDFs, we calculate P_B when $B = 4$, i.e., if the fourth highest SINR value is greater than the threshold pre-processing SINR, α, as we outline in (3.14) and (3.15). For fixed $p = 1$, $q = 1$ and $B = 4$, we obtain the analytical and simulation results for P_B in an urban micro scenario in Fig. 3.3. In the worst case

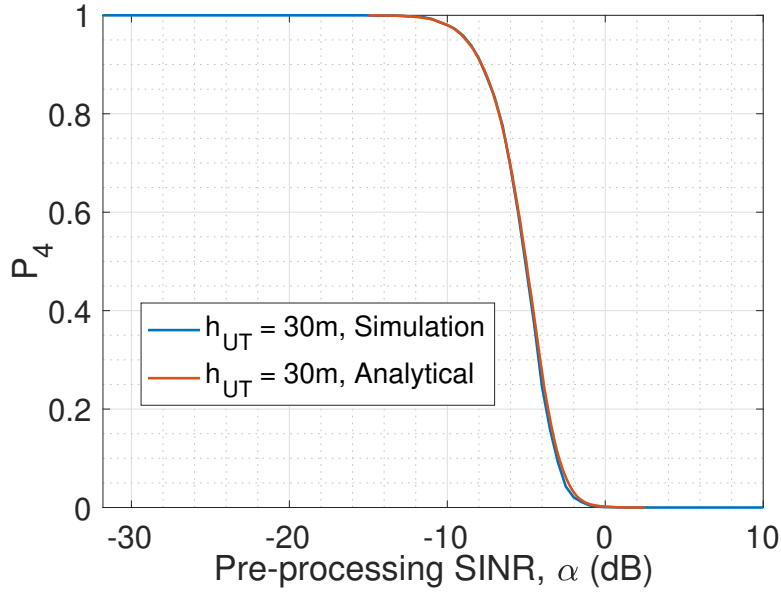

Figure 3.3: P_4 vs. pre-processing SINR threshold α when $p = 1$, $q = 1$ for urban micro scenarios (Reprinted from [2], ©2023 Elsevier, reused with permission).

with no coordination, i.e., $p = 1$, $q = 1$, both participating and non-participating BSs in the network interfere in the localization process. In Fig. 3.3, P_4 is almost one in simulation results at SINR thresholds below -12 dB. This is because a very low threshold constraint at the UAV is achieved easily by the localization signals even in worst-case scenarios with lower received power for the localization signals. We also observe that P_4 becomes almost zero for the SINR threshold greater than 0 dB. This means that without any gain or interference cancellation, it is difficult to achieve the required localizability performance. Since the analytical and the simulation results coincide, our result will depend on the empirical SINR values obtained by our extensive simulations in the following sections.

3.3.2 B-Localizability Performance with Different Number of Participating BSs

In order to analyze B-localizability with a change in the number of participating BSs, we assume a pre-processing SINR threshold of -6 dB [84]. We analyze all the three scenarios to observe the B-localizability for different B values at different altitudes in Fig. 3.4. We observe in the case of the UMi scenario, a B-localizability becomes 0.4 when $h_{UT} = 60$ m and all BSs act as interferers, i.e., $p = 1$, $q = 1$. In general, as we increase the altitude h_{UT}, B-localizability decreases except for

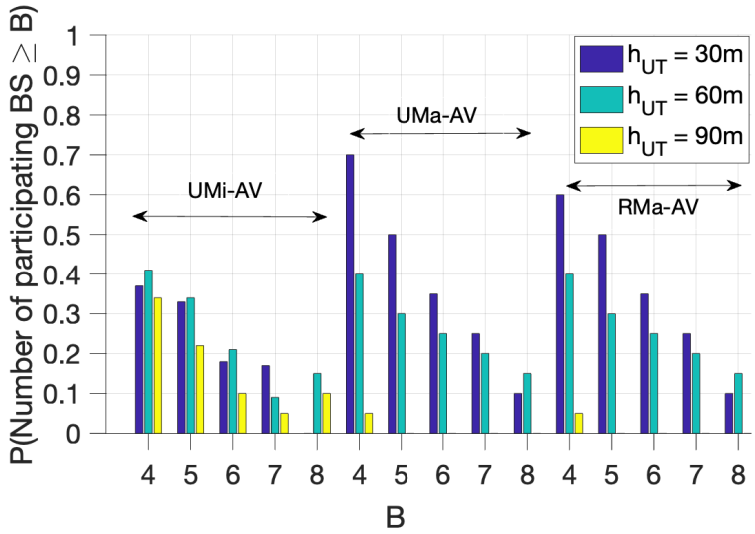

Figure 3.4: P_B vs. number of participating BSs, B, when $p = 1$, $q = 1$ for three different scenarios (Reprinted from [2], ©2023 Elsevier, reused with permission).

certain altitudes like around $h_{UT} = 60$ m for the UMi scenario where localizability increases. This is because of the antenna radiation pattern at the BS which favor certain altitudes. On the other hand, as altitude increases, the higher path loss experienced in the channels becomes dominant, and the localizability performance decreases. The same effect is observed for the urban macro and rural scenarios. As we move from the urban to the rural scenario, the LoS probability increases due to fewer obstacles in the rural area and we observe an increase in the localizability performance. Another interesting observation is that in the case of the UMi scenario, as the number of participating BSs, B, increases, the B-localizability decreases and tends to be zero when $B = 8$ for $h_{UT} = 30$ m. Thus, it becomes impossible to implement a localization method where the required number of participating BSs are eight or more. In the case of the UMa and RMa scenarios, we see that the B-localizability for $h_{UT} = 60$ m and $B = 8$ is higher than in the case of the UMi. Hence with an interference mitigation technique, it is possible to implement localization methods that require a higher number of participating BSs.

3.3.3 Processing Gain Requirement with the Number of Participating BSs

In order to gain some insight into design parameters such as the processing gain at the target UAV, it is important to observe the change in the gain with respect to the

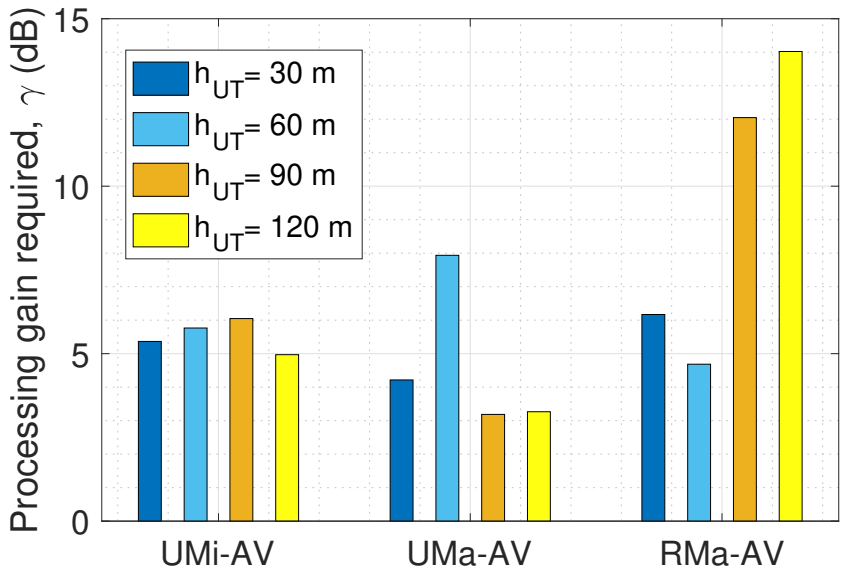

Figure 3.5: Processing gain required for achieving $P_4 = 0.9$ for different altitudes, h_{UT}, when $p = 1$, $q = 1$ for three different scenarios (Reprinted from [2], ©2023 Elsevier, reused with permission).

altitude of the UAV. A sufficient gain provided to the received localization signals can achieve an acceptable P_B. For achieving $P_4 = 0.9$ with an SINR threshold of -6 dB, Fig. 3.5 shows the variation of the gain requirements for different altitudes. We observe that the gain requirement does not follow a trend with the altitude of the UAV. This is because of the antenna gain achieved as a function of the antenna tilt in (3.4) which makes some altitudes favorable for the localization. Fig. 3.5 shows the same analysis for the UMa and RMa scenarios.

We observe that variation in the required gain is small for the urban environment as compared to the rural. Since the wireless channel has almost the same path loss but a different probability of NLoS link conditions in urban areas, the variation in the gain is small. Dynamic allocation of gain with altitude at the receiver can improve localization performance. Based on the altitude and the localization method, the UAV can select the gain to achieve the successful participation of the required number of BSs.

3.3.4 UAV Altitude for Maximum Localizability Performance

As explained in Section 3.2.6, we obtain the dependence of the localizability probability for $B = 4$ on the altitude of the UAV and observe how some of the altitudes

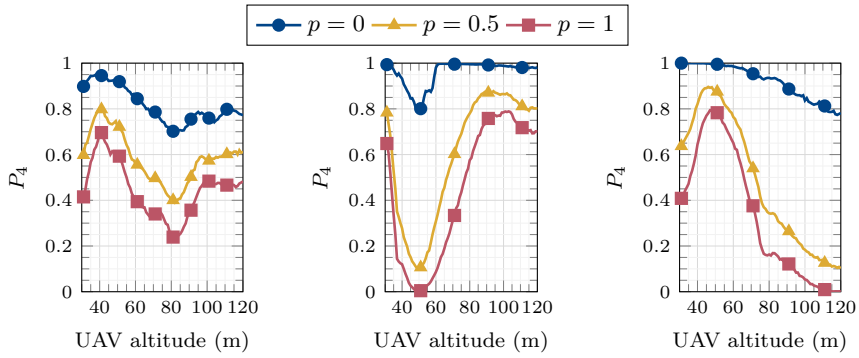

((a)) UMi: ISD = 200 (m) ((b)) UMa: ISD = 500 (m) ((c)) RMa: ISD = 1732 (m)

Figure 3.6: Localizability probability P_4 vs. UAV altitude h_{UT} (m), for different coordination level $p.$, with perfect coordination ($q = 0$, $p = 0$) (Reprinted from [2], ©2023 Elsevier, reused with permission).

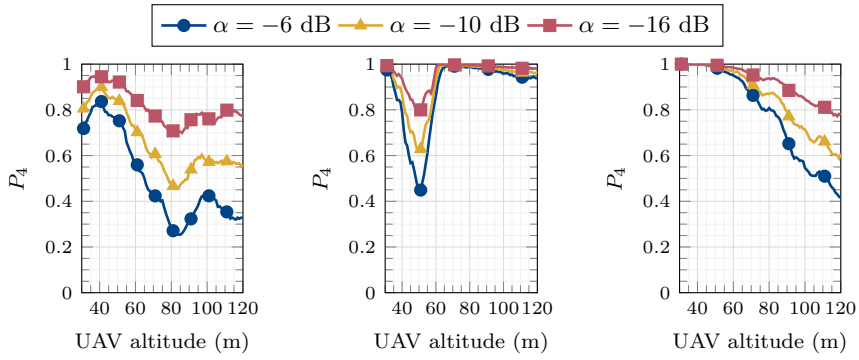

((a)) UMi: ISD = 200 (m) ((b)) UMa: ISD = 500 (m) ((c)) RMa: ISD = 1732 (m)

Figure 3.7: Localizability probability P_4 vs. UAV altitude h_{UT} (m), for different preprocessing SINR (α), with perfect coordination ($q = 0$, $p = 0$) (Reprinted from [2], ©2023 Elsevier, reused with permission).

are more favorable for localization in different scenarios. In Fig. 3.6, we observe the B-localizability for $B = 4$ as a function of UAV altitude h_{UT} for different coordination levels in three different scenarios. In Fig. 3.6(a), we consider the urban micro scenario, Fig. 3.6(b), urban macro scenario, and Fig. 3.6(c), the rural scenario with all the non participating BSs interfering ($q = 1$), while we change the coordination among the participating BSs. We observe for all the scenarios with perfect coordination has the best performance in terms of localizability. For the urban scenarios in 3.6(a), the localizability first increases as the UAV moves up and then decreases before increasing again. This is because of the small inter-site

distance and the antenna pattern at the BSs. Therefore, we have certain altitudes where the localizability performance is highest as in Fig. 3.6(a) for $h_{UT} = 40$ m; Fig. 3.6(b) for $h_{UT} = 90$ m; and Fig. 3.6(c) for $h_{UT} = 50$ m. In the rural scenario, we observe that there is an improvement in the localizability performance and maximum localizability is achieved around $h_{UT} = 50$ for the cases with partial coordination. As the altitude increases, localizability performance decreases for all the coordination (p) values. This is because path loss due to the distance plays a major role as compared to the antenna beam gain.

Fig. 3.7 shows the B-localizability for $B = 4$ as a function of UAV altitude h_{UT} for different pre-processing SINRs (α). We consider the case where we have full coordination among the participating BSs for different pre-processing SINR requirements. We observe that even with perfect coordination, we do not have the best localizability performance at all altitudes. We observe for the urban scenario in Fig. 3.7(a), the performance peaks at around $h_{UT} = 40$ m, showing that the tilt in the BS antennas and the resulting radiation pattern make the altitude range around $h_{UT} = 40$ m favorable for the maximum localizability. For the urban macro scenario in Fig. 3.7(b), we observe a very low localizability probability value at around $h_{UT} = 40 - 50$ m. However, as altitude increases beyond $h_{UT} = 50$ m, localizability experiences a notable improvement, peaking at approximately $h_{UT} = 65$ m. Notably, altitudes exceeding $h_{UT} = 60$ meters exhibit an increased potential for favorable localizability. This is because of the reduction in the density of obstacles at higher altitudes within the urban macro scenario, facilitating LoS A2G links with multiple BSs. In this scenario, the dense distribution of BSs, coupled with perfect coordination, leads to reduced interference from neighboring BSs. Consequently, SINR improves, resulting in enhanced localizability performance. Also, the antenna gain compensates for the inherent path loss that arises due to increased distance. In the rural scenario in Fig. 3.7(c), we do not see the effect of the antenna pattern on the localizability performance because of the large inter-site distances in rural areas where the signal strength is almost the same over the range of the altitudes. The results of Fig. 3.6 and Fig. 3.7 provide us with insights for obtaining maximum localizability results just by changing the operational altitude of the UAV in different scenarios.

3.3.5 Network Coordination and Network Traffic

To illustrate the impact of interference mitigation through network coordination among the B participating BSs, we change the parameter p to vary the level of coordination. This captures the coordination among the participating BSs while non-participating BSs are transmitting, i.e, $q = 1$. In Fig. 3.8(a), considering the UMi scenario with $B = 4$ and a predefined pre-processing SINR threshold, the plot demonstrates an ascending trend in P_4 as the level of coordination (p) intensifies. Heightened coordination, where one BS transmits while others remain idle or transmit on other channels, leads to elevated B-localizability. The enhancement in

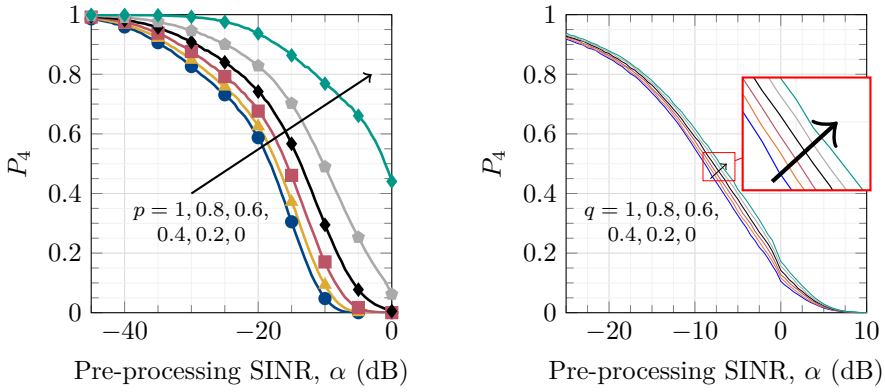

Figure 3.8: P_4 vs. pre-processing SINR threshold, α when $h_{UT} = 30$ m, (a) $q = 1$, and p varying from 1 to 0 with a step of 0.2; (a) $p = 1$, and q varying from 1 to 0 with a step of 0.2 (Reprinted from [2], ©2023 Elsevier, reused with permission).

B-localizability showcases the potential of mitigating interference from neighboring BSs through efficient network coordination.

We explore the impact of traffic among the non-participating BSs by changing q. This parameter encapsulates varying traffic intensities. Setting the parameter q to 1 implies that non-participating BSs are catering to users on the same channel, including other UAVs. This introduces additional interference from these BSs. While $q = 0$ represents perfect coordination among the non-participating BS, resulting in no interference with the target UAV. In Fig. 3.8(b), for the same UMi scenario with $B = 4$, an ascending trend in P_4 is observed as traffic among non-participating BSs decreases. However, the impact of the traffic on localizability is comparatively less substantial than that achieved through network coordination. This result arises from the fact that participating BSs, being in closer proximity with the UAV to be localized, exert a more pronounced impact on SINR compared to non-participating BSs situated at greater distances. Consequently, the effect of non-participating BSs serving more users in the downlink on SINR and localizability is relatively small.

Additionally, we assess the B-localizability performance with $B = 4$ for a UAV in a UMi scenario, as it moves beyond the cellular network's coverage area i.e., away from all the BSs in the two-tier network. The performance results for P_4 are illustrated in Fig. 3.9, depicting its variation with the distance from the central BS, where the BSs have coverage till the distance equal to 2.5 times the ISD. These results are obtained under specific system parameters, including a pre-processing SINR threshold of $\alpha = -16$ dB, $p = 1$, $q = 1$, and $h_{UT} = 40, 80, 120$ m and an ISD = 200 m. At altitudes of 40 m and 80 m for the UAV, P_4 drops to zero as the UAV moves farther away. This is expected since at lower heights, the UAV faces NLoS channels from both nearby and distant BSs. As the distance grows, the

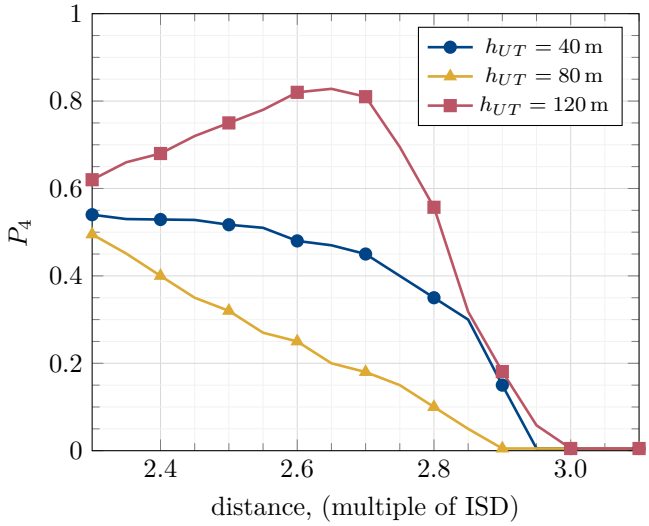

Figure 3.9: P_4 vs. communication distance from the central BS going away from the coverage region of the two-tier cellular network (Reprinted from [2], ©2023 Elsevier, reused with permission).

signal quality diminishes, resulting in a decrease in SINR. Comparing $h_{UT} = 40$ m to $h_{UT} = 80$ m, we find better localizability at the lower altitude, supporting our initial finding that for the UMi scenario, localizability performance at $h_{UT} = 80$ m is very low. At $h_{UT} = 120$ m, an interesting trend emerges: with increasing distance, localizability improves notably. This happens because, at higher altitudes, the UAV usually has a LoS link with most BSs. While moving away, the interference from distant BSs decreases, while the nearest BSs maintain strong signal strength due to a clear LoS channel and full power transmission. This interference reduction boosts the SINR, enhancing localizability.

3.3.6 BS Deployment Model and Communication Frequency

We revisit our assumption that base stations (BSs) are distributed based on a hexagonal grid model. Our objective is to illustrate how this assumption aligns with the localizability outcomes produced by the Poisson Point Process model to show the generalizability of our approach. Fig. 3.10(a) effectively contrasts the localizability outcomes obtained through these random and hexagonal deployment scenarios. This comparison is conducted across varying numbers of participating BSs while maintaining the BS density and constant parameters such as $\alpha = -16$ dB, $h_{UT} = 40$ m, and $p = q = 0$. The variance of shadowing within our channel model is substantial enough to observe a convergence between the hexagonal grid model and the Poisson distribution of BSs. This alignment leads to the convergence

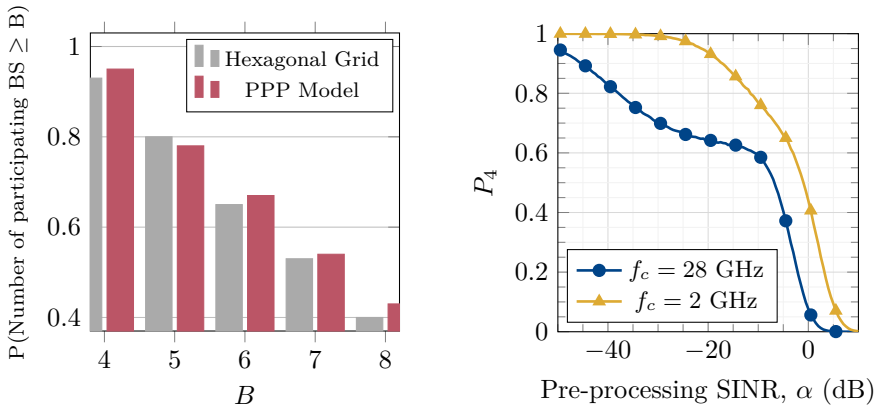

Figure 3.10: Localizability results for an urban micro scenario (a) BS distribution comparison, (b) Frequency range impact (Reprinted from [2], ©2023 Elsevier, reused with permission).

of results from both models.

In Fig. 3.10(b), we compare the localizability under different frequency ranges for $B = 4$. The two frequency ranges being compared are $f_c = 2$ GHz, and $f_c = 28$ GHz. The results for the $f_c = 28$ GHz frequency range are obtained using the channel model provided in [85]. With the perfect coordination in an urban micro scenario, i.e., $p = 0$, $q = 0$, both participating and non-participating BSs in the network do not interfere in the localization process. In Fig. 3.10(b), P_4 shows a difference for the two frequency ranges as the signal at $f_c = 28$ GHz is more susceptible to various losses due to NLoS channel, path loss, and atmospheric absorption. Therefore, the localizability performance is the worst at higher frequency ranges. Nonetheless, a notable advantage stemming from this analysis is that it suggests the possibility of utilizing lower frequency ranges for precise localization while reserving higher frequency ranges for more efficient data transmission purposes.

3.3.7 Model Application: Insights and Limitations

Insights: This localizability analysis represents the initial step towards enabling UAV localization within cellular networks. The localizability metric serves as a valuable tool for designers to measure the ability of the network to localize UAVs and help in selecting optimal localization techniques based on environment, BS deployment, and UAV altitudes. Our findings demonstrate that enhancing localizability performance is achievable through techniques such as processing gain, inter-BS coordination, and strategically operating UAVs within altitude ranges conducive to favorable localizability outcomes across diverse scenarios. For example, we can

gain valuable insights into the ability of a network, utilizing a localization technique reliant on a minimum of four localization signals, to accurately locate a UAV flying at an altitude of 80 meters. For such a case in rural settings with sparsely distributed BSs, its localizability surpasses 80%, indicating effective localization is possible. However, at the same altitude in a densely deployed urban micro scenario, the localizability drops to less than 30%, illustrating challenges in accurate UAV localization with the given method.

Limitations: Our study does not take into account a specific interference avoidance model to accommodate interference coordination schemes. We simplify the control process of interference by coordination through a single parameter. For more specific interference coordination methods, this parameter needs to be updated. However, this simplification effectively captures the influence of interference, albeit without encompassing the precise methods of interference coordination. Also, in our present model, we employ a snapshot approach to calculate localizability. However, there is potential for enhancing the tracking of a moving UAV's position by incorporating its time series location data. Exploring how correlations within the sequential location data can be leveraged to boost localizability performance is a promising avenue for improvement.

3.4 Conclusion

In this chapter, we examine the B-localizability of unmanned aerial vehicles (UAVs) connected to cellular networks, representing the probability of successfully receiving localization signals from at least B participating base stations (BSs) with a signal-to-interference plus noise ratio (SINR) exceeding a specified threshold. Our investigation is grounded in the scenarios defined by 3GPP for cellular-connected UAVs. To assess localizability, we introduce an analytical framework that takes into account both UAV-specific parameters and network-related factors. Monte-Carlo simulations are employed to explore the impact of altitude, the number of participating BSs, and their coordination on localizability. We also analyze the processing gain required to achieve the desired localizability performance. An optimization problem is formulated to maximize localizability and determine the optimal operational altitudes in various scenarios. Our findings indicate that the optimal altitude range for cellular localization varies depending on BS deployments. In scenarios such as the urban micro setting with densely deployed BSs and perfect coordination, the best localizability performance is observed between 30 and 60 meters. Conversely, urban macro environments exhibit optimal performance above 60 meters. The rural scenario, characterized by sparsely deployed BSs and perfect coordination, demonstrates commendable localizability performance across all altitudes.

Chapter 4

Conclusion and Future Work

4.1 Concluding Remarks

The surge in aerial users, particularly cellular-connected UAVs, has spurred interest in academia and industry to enhance existing cellular networks for a more efficient integration of the aerial users. The focus on efficient mobility management and precise localization becomes paramount in achieving this integration. This dissertation addresses the associated research challenges, emphasizing the need for updated mobility management schemes tailored to the unique characteristics of cellular-connected UAVs.

For mobility management, we consider a cellular network which jointly serves the UAVs and the terrestrial users. However, for the UAVs, because of the overlapping coverage of the ground BSs leads to the unnecessary handovers. This not only affects the service continuity but also introduces the delay in the delivery of the uplink data from the UAVs. Thus making it important to update the current mobility management schemes which consider the unique wireless challenges of the UAVs. In order to tackle this challenge and respond to RQ1.1, RQ1.2, and RQ1.2, we formulated a handover decision problem to enhance service availability and reduce unnecessary handovers for cellular-connected UAVs. Two innovative approaches have been introduced to solve the formulated problem. The first employs a model-based strategy utilizing the SA-MRO algorithm, optimizing handover parameters based on buffer queue state information. The second adopts a learning-based method with a model-free DQN algorithm, aiming to improve service availability while minimizing queuing delay and handovers. Both approaches leverage the buffer queue state of the UAV, in addition to signal strength, to make informed handover decisions.

Cellular networks with wide and overlapping coverage in the sky can be used to localize a target UAV with a range based localization technique. In order to answer the research questions RQ2.1, and RQ2.2, we introduce B-localizability which provides valuable insights into UAV localization within cellular networks. The introduced localizability metric serves as a practical tool for designers, guid-

ing the selection of optimal localization techniques based on environmental factors, BS deployment, and UAV altitudes. We provide analytical framework to highlight the significant impact of processing gain, inter-BS coordination, and strategic UAV altitude selection on localizability. We formulated an optimization problem to maximize localizability and determine the optimal operational altitudes in various scenarios. We provide the insights towards the model application and the limitations. Our findings indicate that cellular based localization is an viable option for the UAVs where the optimal altitude range for cellular localization varies depending on BS deployments.

In summary, this dissertation introduces novel mobility management schemes tailored to the unique demands and challenges of the cellular-connected UAVs. Moreover, it introduces a methodology to assess the network's capacity to support range-based localization techniques for UAVs. By addressing these aspects, the research provides valuable insights and potential solutions for the seamless integration of cellular-connected UAVs into existing networks. The findings contribute to the ongoing evolution of network architectures, offering innovative approaches to enhance the performance and adaptability of cellular systems in the presence of UAVs.

4.2 Future Work

Ensuring reliable and fast communication is crucial for controlling cellular-connected UAVs when they operate beyond the visual line of sight. New technologies, like multi-connectivity, where users connect through multiple access points simultaneously, will play a key role. Mobility management is going to be a major challenge in such scenarios. In our earlier work, we concentrated on single connectivity and its mobility management. Now, to build on this and consider multi-connectivity, our upcoming focus is exploring innovative solutions for mobility management solution in such scenarios. Some of the interesting directions for our future work are as follows:

- Advancing Mobility Management in Multi-connectivity Environments:

  In contemporary cell-less wireless networks, users experience a departure from reliance on a single access points (AP) as they are concurrently served in non-orthogonal multiple access scenarios by numerous distributed APs. This shift marks a significant departure from traditional mobility management approaches, moving away from conventional handover management towards a dynamic cluster reconfiguration model. In this evolving paradigm, users can now seamlessly connect with a cluster of distributed APs using the same frequency-time resources. However, adapting this cluster configuration dynamically to suit each user's mobility and meet stringent quality of service (QoS) requirements, including reliability, is essential. Consequently, there is a critical need to explore advanced mobility management strategies in such

multi-connectivity scenarios. Future endeavors can delve into investigating how UAVs can achieve smooth handovers and efficient resource allocation when leveraging multiple base stations simultaneously.

- Adapting to varying reliability requirements: Cellular networks often experience variations in reliability over time or due to service demands. Future research can focus on developing adaptive mechanisms to handle these fluctuations in reliability. This involves dynamic adjustments in handover parameters, resource allocation, and mobility management strategies to ensure consistent and reliable connectivity for UAVs.

- Explainable AI for handover management: Integrating Explainable AI (XAI) techniques can provide transparency and insights into the decision-making process of AI-driven handover management for cellular-connected UAVs. By employing XAI, researchers can delve into the rationale behind handover decisions, making the system more interpretable and facilitating trust among network stakeholders.

Bibliography

[1] I. A. Meer, M. Ozger, D. Schupke, and C. Cavdar, "Mobility management for cellular-connected uavs: Model based versus learning based approaches for service availability," *IEEE Transactions on Network and Service Management*, 2024.

[2] I. A. Meer, M. Ozger, and C. Cavdar, "Cellular localizability of unmanned aerial vehicles," *Vehicular Communications*, vol. 44, p. 100677, 2023.

[3] 3GPP, "Study on Enhanced LTE Support for Aerial Vehicles," 3GPP TR 36.777, Tech. Rep., 2017.

[4] I. A. Meer, W.-H. Lee, M. Ozger, C. Cavdar, and K. W. Sung, "Low-latency mac design for pairwise random networks," in *2022 IEEE 95th Vehicular Technology Conference:(VTC2022-Spring)*. IEEE, 2022, pp. 1–6.

[5] Y. Deng, I. A. Meer, S. Zhang, M. Ozger, and C. Cavdar, "D3qn-based trajectory and handover management for uavs co-existing with terrestrial users," in *2023 21st International Symposium on Modeling and Optimization in Mobile, Ad Hoc, and Wireless Networks (WiOpt)*. IEEE, 2023, pp. 103–110.

[6] M. Ozger, I. Godor, A. Nordlow, T. Heyn, S. Pandi, I. Peterson, A. Viseras, J. Holis, C. Raffelsberger, A. Kercek *et al.*, "6g for connected sky: A vision for integrating terrestrial and non-terrestrial networks," *arXiv preprint arXiv:2305.04271*, 2023.

[7] S. S. S. G. Seeram, S. Zhang, M. Ozger, A. Grabs, J. Holis, and C. Cavdar, "Aerial base stations: Practical considerations for power consumption and service time," in *GLOBECOM 2023-2023 IEEE Global Communications Conference*. IEEE, 2023, pp. 5049–5054.

[8] S. Zhang, T. Cai, D. Wu, D. Schupke, N. Ansari, and C. Cavdar, "Iort data collection with leo satellite-assisted and cache-enabled uav: A deep reinforcement learning approach," *IEEE Transactions on Vehicular Technology*, 2023.

[9] J. Stanczak, I. Z. Kovacs, D. Koziol, J. Wigard, R. Amorim, and H. Nguyen, "Mobility Challenges for Unmanned Aerial Vehicles Connected to Cellular LTE Networks," in *Proc. IEEE VTC Spring*, 2018, pp. 1–5.

[10] J. Chen, M. Ozger, and C. Cavdar, "Nash soft actor-critic leo satellite handover management algorithm for flying vehicles," *arXiv preprint arXiv:2402.00091*, 2024.

[11] Y. Deng, I. A. Meer, S. Zhang, M. Ozger, and C. Cavdar, "D3QN-Based Trajectory and Handover Management for UAVs Co-Existing with Terrestrial Users," in *2023 21st International Symposium on Modeling and Optimization in Mobile, Ad Hoc, and Wireless Networks (WiOpt)*. IEEE, 2023, pp. 103–110.

[12] J. Bai, S.-p. Yeh, F. Xue, and S. Talwar, "Route-aware handover enhancement for drones in cellular networks," in *2019 IEEE Global Communications Conference (GLOBECOM)*. IEEE, 2019, pp. 1–6.

[13] R. Amer, W. Saad, and N. Marchetti, "Mobility in the sky: Performance and mobility analysis for cellular-connected uavs," *IEEE Transactions on Communications*, vol. 68, no. 5, pp. 3229–3246, 2020.

[14] A. Colpaert, E. Vinogradov, and S. Pollin, "3D beamforming and handover analysis for uav networks," in *2020 IEEE Globecom Workshops (GC Wkshps*. IEEE, 2020, pp. 1–6.

[15] S. Euler, H. Maattanen, X. Lin, Z. Zou, M. Bergström, and J. Sedin, "Mobility Support for Cellular Connected Unmanned Aerial Vehicles: Performance and Analysis," in *Proc. IEEE WCNC*, 2019, pp. 1–6.

[16] M. M. U. Chowdhury, W. Saad, and I. Güvenç, "Mobility management for cellular-connected UAVs: A learning-based approach," in *2020 IEEE International Conference on Communications Workshops (ICC Workshops)*. IEEE, 2020, pp. 1–6.

[17] M. M. Azari, A. H. Arani, and F. Rosas, "Mobile cellular-connected UAVs: Reinforcement learning for sky limits," in *2020 IEEE Globecom Workshops (GC Wkshps*. IEEE, 2020, pp. 1–6.

[18] M. L. Marí-Altozano, S. S. Mwanje, S. L. Ramírez, M. Toril, H. Sanneck, and C. Gijón, "A service-centric q-learning algorithm for mobility robustness optimization in lte," *IEEE Transactions on Network and Service Management*, vol. 18, no. 3, pp. 3541–3555, 2021.

[19] A. Madelkhanova, Z. Becvar, and T. Spyropoulos, "Q-learning-based setting of cell individual offset for handover of flying base stations," in *2022 IEEE 95th Vehicular Technology Conference:(VTC2022-Spring)*. IEEE, 2022, pp. 1–7.

[20] A. Lobinger, S. Stefanski, T. Jansen, and I. Balan, "Load balancing in downlink LTE self-optimizing networks," in *2010 IEEE 71st vehicular technology conference*. IEEE, 2010, pp. 1–5.

[21] N. O. Tuncel and M. Koca, "Joint ICIC and mobility management optimization in self-organizing networks," in *2017 IEEE Wireless Communications and Networking Conference (WCNC)*. IEEE, 2017, pp. 1–6.

[22] B. Galkin, E. Fonseca, R. Amer, L. A. DaSilva, and I. Dusparic, "Reqiba: Regression and deep q-learning for intelligent uav cellular user to base station association," *IEEE Transactions on Vehicular Technology*, vol. 71, no. 1, pp. 5–20, 2021.

[23] Y. Chen, X. Lin, T. Khan, and M. Mozaffari, "Efficient drone mobility support using reinforcement learning," in *2020 IEEE wireless communications and networking conference (WCNC)*. IEEE, 2020, pp. 1–6.

[24] V. Yajnanarayana, H. Rydén, and L. Hévizi, "5G handover using reinforcement learning," in *2020 IEEE 3rd 5G World Forum (5GWF)*. IEEE, 2020, pp. 349–354.

[25] A. Azari, F. Ghavimi, M. Ozger, R. Jantti, and C. Cavdar, "Machine Learning assisted Handover and Resource Management for Cellular Connected Drones," in *Proc. IEEE VTC-Spring*, 2020.

[26] Y. Jang, S. M. Raza, M. Kim, and H. Choo, "Proactive handover decision for UAVs with deep reinforcement learning," *Sensors*, vol. 22, no. 3, p. 1200, 2022.

[27] K. Dimou, M. Wang, Y. Yang, M. Kazmi, A. Larmo, J. Pettersson, W. Muller, and Y. Timner, "Handover within 3GPP LTE: Design principles and performance," in *Proc IEEE VTC-Fall*, 2009, pp. 1–5.

[28] A. Lobinger, S. Stefanski, T. Jansen, and I. Balan, "Coordinating handover parameter optimization and load balancing in LTE self-optimizing networks," in *Proc IEEE VTC-Spring*, 2011, pp. 1–5.

[29] I. M. Bălan, B. Sas, T. Jansen, I. Moerman, K. Spaey, and P. Demeester, "An enhanced weighted performance-based handover parameter optimization algorithm for LTE networks," *EURASIP Journal on Wireless Communications and Networking*, vol. 2011, no. 1, pp. 1–11, 2011.

[30] V. Buenestado, J. M. Ruiz-Aviles, M. Toril, and S. Luna-Ramirez, "Mobility robustness optimization in enterprise lte femtocells," in *2013 IEEE 77th Vehicular Technology Conference (VTC Spring)*. IEEE, 2013, pp. 1–5.

[31] Y.-W. Mal, J.-L. Chen, and H.-K. Lin, "Mobility robustness optimization based on radio link failure prediction," in *2018 Tenth International Conference on Ubiquitous and Future Networks (ICUFN)*. IEEE, 2018, pp. 454–457.

[32] "A survey on radio frequency based precise localisation technology for UAV in GPS-denied environment," *Journal of Intelligent & Robotic Systems*, vol. 103, no. 3, pp. 1–30, 2021.

[33] V. Walter, M. Saska, and A. Franchi, "Fast Mutual Relative Localization of UAVs using Ultraviolet LED Markers," in *Proc. IEEE International Conference on Unmanned Aircraft Systems (ICUAS)*, 2018, pp. 1217–26.

[34] J. Wan, L. Zhong, and F. Zhang, "Cooperative Localization of Multi-UAVs via Dynamic Nonparametric Belief Propagation under GPS Signal Loss Condition," *Hindawi International Journal of Distributed Sensor Networks*, vol. 2014, pp. 1–10, 2014.

[35] Y. Dobrev *et al.*, "Radar-Based High-Accuracy 3D Localization of UAVs for Landing in GNSS-Denied Environments," in *Proc. MTT-S International Conference on Microwaves for Intelligent Mobility (ICMIM)*, 2018, pp. 1–4.

[36] P. Sinha and I. Guvenc, "Impact of antenna pattern on toa based 3d uav localization using a terrestrial sensor network," *IEEE Transactions on Vehicular Technology*, vol. 71, no. 7, pp. 7703–7718, 2022.

[37] S. Chang, Y. Zheng, P. An, J. Bao, and J. Li, "3-d rss-aoa based target localization method in wireless sensor networks using convex relaxation," *IEEE Access*, vol. 8, pp. 106 901–106 909, 2020.

[38] Q. Wang, Z. Duan, and X. R. Li, "Three-dimensional location estimation using biased rss measurements," *IEEE Transactions on Aerospace and Electronic Systems*, vol. 56, no. 6, pp. 4673–4688, 2020.

[39] S. Tomic, M. Beko, and R. Dinis, "3-d target localization in wireless sensor networks using rss and aoa measurements," *IEEE Transactions on Vehicular Technology*, vol. 66, no. 4, pp. 3197–3210, 2016.

[40] Y. Li, F. Shu, B. Shi, X. Cheng, Y. Song, and J. Wang, "Enhanced rss-based uav localization via trajectory and multi-base stations," *IEEE Communications Letters*, vol. 25, no. 6, pp. 1881–1885, 2021.

[41] J. Schloemann, H. S. Dhillon, and R. M. Buehrer, "Toward a tractable analysis of localization fundamentals in cellular networks," *IEEE Transactions on Wireless Communications*, vol. 15, no. 3, pp. 1768–1782, 2015.

[42] F. Tong, Y. Sun, and S. He, "On Positioning Performance for the Narrow-Band Internet of Things: How Participating eNBs Impact?" *IEEE Transactions on Industrial Informatics*, vol. 15, no. 1, pp. 423–433, 2018.

[43] I. A. Meer, M. Ozger, and C. Cavdar, "On the Localization of Unmanned Aerial Vehicles with Cellular Networks," in *Proc. IEEE WCNC*, 2020, pp. 1–6.

[44] E. Dinc, M. Vondra, and C. Cavdar, "Total cost of ownership optimization for direct air-to-ground communication networks," *IEEE Transactions on Vehicular Technology*, vol. 70, no. 10, pp. 10 157–10 172, 2021.

[45] ——, "Multi-user beamforming and ground station deployment for 5g direct air-to-ground communication," in *GLOBECOM 2017-2017 IEEE Global Communications Conference*. IEEE, 2017, pp. 1–7.

[46] D. Tomić, S. Hofmann, M. Ozger, D. Schupke, and C. Cavdar, "Quality of service aware traffic management for aircraft communications," in *2020 IEEE 91st Vehicular Technology Conference (VTC2020-Spring)*. IEEE, 2020, pp. 1–6.

[47] E. Dinc, M. Vondra, S. Hofmann, D. Schupke, M. Prytz, S. Bovelli, M. Frodigh, J. Zander, and C. Cavdar, "In-flight broadband connectivity: Architectures and business models for high capacity air-to-ground communications," *IEEE Communications Magazine*, vol. 55, no. 9, pp. 142–149, 2017.

[48] E. Dinc, M. Vondra, and C. Cavdar, "Seamless gate-to-gate connectivity concept: Onboard lte, wi-fi and laa," in *2017 IEEE 86th Vehicular Technology Conference (VTC-Fall)*. IEEE, 2017, pp. 1–7.

[49] A. E. Garcia, M. Ozger, A. Baltaci, S. Hofmann, D. Gera, M. Nilson, C. Cavdar, and D. Schupke, "Direct air to ground communications for flying vehicles: Measurement and scaling study for 5g," in *2019 IEEE 2nd 5G World Forum (5GWF)*. IEEE, 2019, pp. 310–315.

[50] V. Megas, S. Hoppe, M. Ozger, D. Schupke, and C. Cavdar, "A combined topology formation and rate allocation algorithm for aeronautical ad hoc networks," *IEEE Transactions on Mobile Computing*, 2022.

[51] M. Vondra, E. Dinc, M. Prytz, M. Frodigh, D. Schupke, M. Nilson, S. Hofmann, and C. Cavdar, "Performance study on seamless da2gc for aircraft passengers toward 5g," *IEEE Communications Magazine*, vol. 55, no. 11, pp. 194–201, 2017.

[52] M. Vondra, M. Ozger, D. Schupke, and C. Cavdar, "Integration of satellite and aerial communications for heterogeneous flying vehicles," *Ieee network*, vol. 32, no. 5, pp. 62–69, 2018.

[53] 3GPP TR 36.777, "Enhanced LTE support for aerial vehicles," Tech. Rep., 2018. [Online]. Available: ftp://www.3gpp.org

[54] A. Fakhreddine *et al.*, "Handover challenges for cellular-connected drones," in *ACM 5th Workshop on Micro Aerial Vehicle Networks, Systems, and Applications*, 2019.

[55] A. Baltaci, H. Cech, N. Mohan, F. Geyer, V. Bajpai, J. Ott, and D. Schupke, "Analyzing real-time video delivery over cellular networks for remote piloting aerial vehicles," in *Proceedings of the 22nd ACM Internet Measurement Conference*, 2022, pp. 98–112.

[56] A. Baltaci, E. Dinc, M. Ozger, A. Alabbasi, C. Cavdar, and D. Schupke, "A survey of wireless networks for future aerial communications (facom)," *IEEE Communications Surveys & Tutorials*, 2021.

[57] O-RAN Alliance, "O-RAN: Towards an Open and Smart RAN," Tech. Rep., 2018. [Online]. Available: https://www.o-ran.org/resources

[58] A. Lacava *et al.*, "Programmable and Customized Intelligence for Traffic Steering in 5G Networks Using Open RAN Architectures," *arXiv preprint arXiv:2209.14171v3*, 2022.

[59] M. Polese, L. Bonati, S. D'Oro, S. Basagni, and T. Melodia, "Understanding O-RAN: architecture, interfaces, algorithms, security, and research challenges," *CoRR*, vol. abs/2202.01032, 2022. [Online]. Available: https://arxiv.org/abs/2202.01032

[60] F. Salehi, M. Ozger, N. Neda, and C. Cavdar, "Ultra-reliable low-latency communication for aerial vehicles via multi-connectivity," in *2022 Joint European Conference on Networks and Communications & 6G Summit (EuCNC/6G Summit)*. IEEE, 2022, pp. 166–171.

[61] M. Kalil *et al.*, "Low-Complexity Power-Efficient Schedulers for LTE Uplink With Delay-Sensitive Traffic," *IEEE Trans. Veh. Technol*, vol. 64, no. 10, pp. 4551–4564, 10 2015.

[62] F. Salehi, M. Ozger, and C. Cavdar, "Reliability and delay analysis of 3-dimensional networks with multi-connectivity: Satellite, haps, and cellular communications," *IEEE Transactions on Network and Service Management*, 2023.

[63] M. I. Ashraf, C.-F. Liu, M. Bennis, W. Saad, and C. S. Hong, "Dynamic resource allocation for optimized latency and reliability in vehicular networks," *IEEE Access*, vol. 6, pp. 63 843–63 858, 2018.

[64] ICAO, "Aeronautical Telecommunication Network (ATN) Manual for the ATN Using IPS Standards and Protocols Draft Version 21," Tech. Rep. Doc 9896, 2012.

[65] NGMN, "Verticals uRLLC Use Cases and Requirements by NGMN Alliance," Tech. Rep., 2020.

[66] V. Mnih *et al.*, "Human-level control through deep reinforcement learning," *Nature*, vol. 518, no. 7540, p. 529, 2015.

[67] M. T. Nguyen, S. Kwon, and H. Kim, "Mobility robustness optimization for handover failure reduction in lte small-cell networks," *IEEE Transactions on Vehicular Technology*, vol. 67, no. 5, pp. 4672–4676, 2017.

[68] M. Ozger, M. Vondra, and C. Cavdar, "Towards beyond Visual Line of Sight Piloting of UAVs with Ultra Reliable Low Latency Communication," in *Proc. IEEE GLOBECOM*, Dec 2018, pp. 1–6.

[69] I. A. Meer, M. Ozger, M. Lundmark, K. W. Sung, and C. Cavdar, "Ground Based Sense and Avoid System for Air Traffic Management," in *Proc. IEEE PIMRC*, 2019, pp. 1–6.

[70] P. Sinha, Y. Yapici, and I. Guvenc, "Impact of 3D Antenna Radiation Patterns on TDOA-Based Wireless Localization of UAVs," in *Proc. IEEE INFOCOM WKSHPS*, 2019, pp. 614–619.

[71] X. Lin, V. Yajnanarayana, S. D. Muruganathan, S. Gao, H. Asplund, H.-L. Maattanen, M. Bergstrom, S. Euler, and Y.-P. E. Wang, "The sky is not the limit: LTE for unmanned aerial vehicles," *IEEE Communications Magazine*, vol. 56, no. 4, pp. 204–210, 2018.

[72] M. M. Azari, F. Rosas, A. Chiumento, and S. Pollin, "Coexistence of terrestrial and aerial users in cellular networks," in *Proc. IEEE GLOBECOM Workshops (GC Wkshps)*, 2017, pp. 1–6.

[73] T. Wang, H. Xiong, H. Ding, and L. Zheng, "TDOA-based joint synchronization and localization algorithm for asynchronous wireless sensor networks," *IEEE Transactions on Communications*, vol. 68, no. 5, pp. 3107–3124, 2020.

[74] H. Tabassum, M. Salehi, and E. Hossain, "Fundamentals of mobility-aware performance characterization of cellular networks: A tutorial," *IEEE Communications Surveys & Tutorials*, vol. 21, no. 3, pp. 2288–2308, 2019.

[75] C. Laoudias, A. Moreira, S. Kim, S. Lee, L. Wirola, and C. Fischione, "A survey of enabling technologies for network localization, tracking, and navigation," *IEEE Communications Surveys & Tutorials*, vol. 20, no. 4, pp. 3607–3644, 2018.

[76] V. Jungnickel, T. Wirth, M. Schellmann, T. Haustein, and W. Zirwas, "Synchronization of cooperative base stations," in *2008 IEEE International Symposium on Wireless Communication Systems*. IEEE, 2008, pp. 329–334.

[77] S. Hu, A. Berg, X. Li, and F. Rusek, "Improving the performance of OTDOA based positioning in NB-IoT systems," in *Proc. IEEE Global Communications Conference (GLOBECOM)*, 2017, pp. 1–7.

[78] J. C. Eidson, M. Fischer, and J. White, "Ieee-1588™ standard for a precision clock synchronization protocol for networked measurement and control systems," in *Proceedings of the 34th Annual Precise Time and Time Interval Systems and Applications Meeting*, 2002, pp. 243–254.

[79] 3GPP, "Study on NR positioning support," 3GPP TR 38.855 , Tech. Rep., 2019.

[80] Yang, Chao and Mao, Shiwen and Wang, Xuyu, "An Overview of 3GPP Positioning Standards," *GetMobile: Mobile Computing and Communications*, vol. 26, no. 1, pp. 9–13, 2022.

[81] Yang, C and Mao, S and Wang X, "An Overview of 3GPP Positioning Standards," *ACM GetMobile: Mobile Comp. and Comm.*, vol. 26, no. 1, pp. 9–13, 2022.

[82] M. Ahmadi and J. Pan, "Random distances associated with arbitrary triangles: A recursive approach with an arbitrary reference point," Tech. Rep., University of Victoria-2013.

[83] D. Tse and P. Viswanath, *Fundamentals of wireless communication*. Cambridge university press, 2005.

[84] J. Schloemann, H. S. Dhillon, and R. M. Buehrer, "Localization performance in cellular networks," in *Proc. IEEE International Conference on Communication Workshop (ICCW)*, 2015, pp. 871–876.

[85] P. Wang, M. Ozger, C. Cavdar, and M. Petrova, "Beyond visual line of sight piloting of UAVs using millimeter-wave cellular networks," in *2019 IEEE 30th Annual International Symposium on Personal, Indoor and Mobile Radio Communications (PIMRC)*. IEEE, 2019, pp. 1–7.